Acta Pharmacologica Sinica

www.nature.com/aps

ARTICLE

Cardiomyocyte OTUD7b drives diabetic cardiomyopathy via deubiquitinating and stabilizing TAK1

Xue Han[1,2], Guo-xuan Liu[1], Jia-ning Zheng[1], Ming-yang He[1], Li Zhuang[1], Jia-jia Zhang[1], Jie Tong[1,2], Zhu-qi Huang[2], Yu-rou Wu[1], Tong-qing Zhou[1], Ju-lin Min[3], Ze-ping Zhang[3], Ning Zhu[4], Qiao-juan Shi[1], Wen-bing Jiang[4]✉, Hua-zhong Ying[1]✉ and Guang Liang[1,2,3]✉

Deubiquitinating enzymes (DUBs) are critically involved in diabetic cardiomyopathy (DCM), yet the function of OTU domain-containing protein 7B (OTUD7b), a recently identified DUB, in DCM remains unknown. Here, we identified that OTUD7b expression was significantly elevated in cardiomyocytes from both type 1 and type 2 diabetic mouse hearts. Cardiomyocyte-specific deletion of OTUD7b ameliorated cardiac dysfunction, hypertrophy, and fibrosis in diabetic mice, without affecting systemic hyperglycemia. Mechanistically, combining ubiquitinome and interactome analyses, we identified transforming growth factor β-activated kinase 1 (TAK1) as a direct substrate of OTUD7b in cardiomyocytes. Under diabetic conditions, OTUD7b binds to TAK1 via its zinc finger domain and catalyzes K48-linked deubiquitination at the K346 of TAK1, thereby enhancing TAK1 protein stability. This OTUD7b-mediated stabilization increased the levels of both TAK1 and p-TAK1, which led to hyperactivation of the TAK1-MAPK (JNK/p38) axis, subsequently promoting extrinsic apoptosis and inflammatory responses in cardiomyocytes. Crucially, cardiomyocyte-specific reconstitution of a deubiquitination-resistant TAK1-K346R mutant in diabetic mice completely abolished the cardioprotective effects of OTUD7b deficiency, confirming that OTUD7b drives DCM primarily through deubiquitinating TAK1 at K346. Taken together, our study unveils a novel OTUD7b-TAK1 axis in cardiomyocytes driving diabetic heart injury and positions OTUD7b as a promising therapeutic target for DCM.

Keywords: diabetic cardiomyopathy; deubiquitinating enzyme; OTUD7b; TAK1; apoptosis; inflammation

Acta Pharmacologica Sinica (2026) 0:1–17; https://doi.org/10.1038/s41401-026-01891-w

INTRODUCTION

Diabetic cardiomyopathy (DCM) represents a distinct myocardial disorder that arises independently of hypertension, coronary artery disease, or valvular pathology [1, 2]. It is a major contributor to heart failure (HF) in diabetic populations and carries a disproportionately high risk of mortality [3]. Despite widespread clinical use of conventional cardioprotective agents such as angiotensin-converting enzyme inhibitors, angiotensin receptor blockers, and beta blockers in diabetic populations, there remains a paucity of evidence supporting their efficacy specifically for DCM [4, 5]. Therefore, deciphering the underlying mechanisms of DCM is imperative to identify new and effective targeted therapies for this disease.

As the fundamentally functional units of the heart, cardiomyocytes are not merely passive targets of metabolic insult but active orchestrators of pathological remodeling [5]. Chronic hyperglycemia and dyslipidemia reprogram cardiomyocyte function by sensitizing these cells to extrinsic apoptotic triggers such as Fas ligand (FasL), which activates caspase 8 and caspase 3 to induce apoptosis [6]. Compared with non-diabetic individuals, cardiomyocyte apoptosis is reported to be approximately 85-fold higher in diabetic patients [7], contributing to myocardial remodeling, contractile dysfunction, and even HF. Beyond apoptosis, diabetes-induced inflammatory processes act synergistically to exacerbate myocardial injury and promote functional deterioration in cardiomyocytes. Within the inflammatory network, cardiomyocytes are not merely passive victims but active participants, regulators, and signaling hubs [8, 9]. Under hyperglycemic conditions, injured cardiomyocytes release pro-inflammatory cytokines, such as tumor necrosis factor-alpha (TNF-α) and interleukin-6 (IL-6), and danger-associated molecular patterns (DAMPs), which subsequently activate the nuclear factor kappa B (NF-κB) and mitogen-activated protein kinases (MAPK) signaling pathways. This activation amplifies inflammatory cascades and orchestrates immune cell recruitment, thereby establishing a sustained pro-inflammatory and pro-apoptotic environment [9–11]. Transforming growth factor-β–activated kinase 1 (TAK1) serves as a pivotal upstream regulator that integrates multiple apoptotic and inflammatory signals in cardiomyocytes [12]. Studies in diabetic mice have demonstrated that elevated TAK1 activity is associated with enhanced apoptotic and inflammatory responses in cardiomyocytes, leading to progressive deterioration of cardiac function [13–15]. Therefore, targeting the key regulators governing cardiomyocyte fate, such as TAK1, may represent a promising therapeutic strategy for DCM.

[1]Zhejiang Provincial Key Laboratory of Drug Discovery and Safety Evaluation for Inflammatory Chronic Diseases, Laboratory Animal Center, Hangzhou Medical College, Hangzhou 310007, China; [2]Zhejiang-Thailand International Joint Laboratory for Cardiovascular Disease Research, School of Pharmaceutical Sciences, Hangzhou Medical College, Hangzhou 310007, China; [3]Department of Cardiology, the First Affiliated Hospital, Wenzhou Medical University, Wenzhou 325035, China and [4]Department of Cardiology, Affiliated Wenzhou People's Hospital, Hangzhou Medical College, Wenzhou 325000, China
Correspondence: Wen-bing Jiang (jiangwb919@wmu.edu.cn) or Hua-zhong Ying (yhz0101@126.com) or Guang Liang (wzmcliangguang@163.com)

Received: 7 April 2026 Accepted: 6 July 2026
Published online: 03 August 2026

Posttranslational modifications, particularly ubiquitination and deubiquitination, play pivotal roles in regulating protein stability, localization, and activity in disease contexts [16]. The process of deubiquitination is mediated by deubiquitinating enzymes (DUBs), which remove ubiquitin molecules from substrate proteins [17]. Ovarian tumor domain-containing 7b (OTUD7b), a member of the ovarian tumor-related proteases (OTU) family in DUBs, features a catalytic OTU domain, a ubiquitin-associated domain (UBA) domain, and a zinc finger (ZF) domain. It selectively cleaves K11-, K48-, and K63-linked polyubiquitin chains, and is known to regulate cancer progression, immune responses, and inflammatory disorders [18–21]. For instance, OTUD7b promotes p53-dependent apoptosis in hepatocellular carcinoma [19], while also regulating inflammatory responses and cell survival signaling via the deubiquitination of TRAF3 and RIPK1 in lung cancer and encephalomyelitis [21, 22]. Recent findings also suggest a role of OTUD7b in pressure-overload-induced cardiac hypertrophy [23, 24]. However, its involvement in DCM has never been systematically investigated.

In this study, we found that OTUD7b expression was significantly elevated in cardiomyocytes from both type 1 and type 2 diabetic mouse hearts. Cardiomyocyte-specific OTUD7b deficiency effectively prevented DCM in diabetic mice. Mechanistically, OTUD7b stabilized TAK1 by removing K48-linked polyubiquitin chains at the K346 residue, thereby increasing TAK1 levels and promoting activation of the TAK1-MAPK axis, inducing inflammation and apoptosis in cardiomyocytes. Our study revealed a previously unrecognized detrimental role of OTUD7b in diabetic hearts and identified a cardiomyocyte-specific OTUD7b-TAK1 axis that mediates DCM, suggesting that targeting OTUD7b represents a potential therapeutic strategy for DCM.

MATERIALS AND METHODS

Animals

All animal experiments strictly adhered to the guidelines of the National Institutes of Health (NIH, USA). Experimental protocols were approved by the Ethics Committee for Laboratory Animal Care and Welfare of Hangzhou Medical College (Approval No. ZJCLA-IACUC-20010562; Hangzhou, China). Cardiomyocyte-specific OTUD7b-knockout mice were generated in collaboration with GemPharmatech (Nanjing, China). The generation protocol was as follows: *Otud7b*$^{fl/fl}$ mice (C57BL/6JGpt-*Otud7b*^{em1Cflox}/Gpt, strain No. T008065) were crossed with α-myosin heavy chain promoter-driven heterozygous Cre mice (Myh6-Cre, C57BL/6JGpt-*H11*$^{em1Cin(Myh6\text{-}CreERT2)}$/Gpt) to produce cardiomyocyte-specific OTUD7b-knockout mice. *Otud7b*$^{fl/fl}$ littermate mice were used as the control group. All mice were maintained in specific pathogen-free facilities under controlled environmental conditions (temperature: 20–25 °C; humidity: 50% ± 10%) with a 12-h light/dark cycle. Food and water were available *ad libitum*.

Animal experiments

All animal procedures in this study were conducted following the principles of randomization and blinding. Male mice were selected for all animal experiments in the current study. Mice were allowed a two-week acclimatization period before the commencement of the experiment.

The type 2 diabetes mellitus (T2DM) mouse model was induced by HFD combined with STZ injection as previously reported [25]. OTUD7b gene deletion in mice was induced by tamoxifen (75 mg/kg, *i.p.*) injection for five consecutive days. Eight-week-old male *Otud7b* CKO mice and the littermate *Otud7b*$^{fl/fl}$ mice were randomly divided into 4 experimental groups ($n = 6$): *Otud7b*$^{fl/fl}$-sham group, *Otud7b* CKO-sham group, *Otud7b*$^{fl/fl}$-T2DM group and *Otud7b* CKO-T2DM group. After eight weeks of HFD containing 60.3 kcal% fat (D12492, Research Diets, New Brunswick, USA), the mice received intraperitoneal injections of 35 mg/kg STZ (1883664, Sigma-Aldrich, St Louis, USA) in citrate buffer once daily for three consecutive days. Mice were maintained on HFD for an additional eight weeks. Control mice were fed a normal diet (10 kcal% fat) and administered an equivalent volume of citrate buffer via intraperitoneal injection.

For the type 1 diabetes mellitus (T1DM) mouse model, eight-week-old male *Otud7b* CKO mice and the littermate *Otud7b*$^{fl/fl}$ mice were randomly divided into 4 experimental groups ($n = 6$ in each group): *Otud7b*$^{fl/fl}$-sham group, *Otud7b* CKO-sham group, *Otud7b*$^{fl/fl}$-T1DM group and *Otud7b* CKO-T1DM group. The mice received intraperitoneal injections of STZ at a dose of 60 mg/kg for three consecutive days and were subsequently maintained for 16 weeks. Mice in the sham groups were administered an equivalent volume of sodium citrate buffer (pH 4.5) via intraperitoneal injection.

Blood glucose levels and body weight were measured weekly at consistent time points. Diabetic mice were considered successfully modeled when fasting blood glucose (FBG) levels exceeded 12 mmol/L. At the end of the animal studies, mice were euthanized via intraperitoneal injection of pentobarbital sodium (40 mg/kg) and sacrificed through cervical dislocation. Blood samples and cardiac tissues were harvested for further analysis. Active caspase 8 in heart tissues was quantified using a caspase activity assay kit (C1152, Beyotime Biotechnology, Shanghai, China) according to the manufacturer's instructions.

Echocardiography

Cardiac function in mice was evaluated by transthoracic echocardiography using an ultrasound diagnostic system (D6VET, VINNO, Suzhou, China). Mice were anesthetized with 2%–2.5% isoflurane via inhalation. When the hind paw withdrawal reflex was absent, the isoflurane concentration was reduced to 1.0%–1.5% to maintain a heart rate of approximately 450 beats per minute. Then, the echocardiogram of the mouse was grabbed. Diastolic function at the mitral valve level was assessed using pulsed wave and tissue Doppler imaging after acquiring the apical four-chamber view. All evaluation parameters were measured using two-dimensional M-mode echocardiography over at least five consecutive cardiac cycles. The left ventricular end-systolic diameter (LVID), left ventricular end-systolic volume (LVESV), and LVIDd were utilized to assess the systolic function of the left ventricle in mice. The EF and FS were calculated using the following formulas: EF = [(end-diastolic volume - end-systolic volume)/end-diastolic volume] × 100%, FS = [(LVIDd - LVID) / LVIDd] × 100%.

Heart tissues staining

Mice cardiac tissues were harvested, fixed with 4% paraformaldehyde solution overnight, and subsequently embedded in paraffin. The samples were sectioned transversely into 5 μm thick slices using a sliding microtome (Leica, Wetzlar, Germany). Tissue sections were deparaffinized with xylene and rehydrated through a series of ethanol washes. Hematoxylin and Eosin (H&E) (G1120, Solarbio Life Sciences, Beijing, China) staining was used to evaluate the histopathological damage of the mouse heart. Sirius Red (G3632, Solarbio Life Sciences) staining and Masson's Trichrome (G1340, Solarbio Life Sciences) were used to evaluate cardiac fibrosis and collagen deposition. After staining, stained images of all heart tissue samples were captured under random fields using an optical microscope (200× magnification; Leica) and subsequently analyzed using ImageJ software (National Institutes of Health, Bethesda, USA).

For wheat germ agglutinin (WGA) staining, paraffin-embedded heart sections were stained with the WGA staining kit (C1610, Solarbio Life Sciences) to evaluate the cross-sectional area of cardiomyocytes. Images were acquired using a fluorescence microscope under random fields, and the cross-sectional area of cardiomyocytes was quantified using ImageJ software (National Institutes of Health, USA).

For TUNEL staining, paraffin-embedded cardiac sections were processed according to the manufacturer's protocol for the One-

Step TUNEL Apoptosis Detection Kit (C1090, Beyotime Biotechnology). Fluorescence images were captured from randomly selected fields, and the numbers of TUNEL-positive and total nuclei were counted in each field. The percentage of TUNEL-positive cells was calculated and subjected to statistical analysis.

Paraffin-embedded cardiac sections were stained for cleaved-caspase 3 using the SignalStain Apoptosis (Cleaved-caspase 3) IHC Detection Kit (12692, Cell Signaling Technology, Massachusetts, USA), following the manufacturer's instructions.

For cardiac tissue immunofluorescence assays, the tyramide signal amplification kit (TSA kit; RC0086Plus-34R, Record Biological Technology Co., Ltd., Shanghai, China) was used for fluorescent staining of paraffin sections. Immunofluorescence staining was carried out in strict accordance with the manufacturer's instructions. The primary antibodies used in this study were incubated overnight at 4 °C and included OTUD7b (1:200; 16605-1-AP, Proteintech, Wuhan, China), CD68 (1:200; 25747-1-AP, Proteintech), α-actinin (1:200; ab9465, Abcam, Cambridge, UK), and vimentin (1:400; ab8978, Abcam). The TSA fluorescent dye reaction solution was applied, followed by incubation with DAPI at room temperature for 15 min in the dark. The sections were then mounted for analysis. Images were captured using a confocal fluorescence microscope (Nikon, Tokyo, Japan) at 400× magnification, and subsequent image analysis was performed using ImageJ software.

TRITC-Phalloidin staining

To investigate the correlation between cell morphology and function in the context of myocardial injury, TRITC-Phalloidin staining was employed to assess the morphological changes in NRPCs subjected to high-glucose-induced damage. NRPCs were seeded at an appropriate density onto 24-well plates containing glass coverslips, washed three times with sterile PBS pre-warmed to 37°C, and then fixed with 4% paraformaldehyde solution at room temperature for 20 min. Following the removal of residual paraformaldehyde by washing with PBS, the cell membrane was permeabilized using 0.1% Triton X-100 for 5 min. Subsequently, the cells were stained with Actin-Tracker Red (C2205S, Beyotime Biotechnology) for 1 h in the dark. The nuclei were counterstained with DAPI (C0065, Solarbio Life Sciences), and excess dye was removed by washing with PBS. To preserve fluorescence signals, the samples were mounted using an anti-fade mounting medium. Cell images were captured using the Nikon fluorescence microscope at 400× magnification.

Cellular immunofluorescence staining

Cellular immunofluorescence staining was performed to assess the colocalization of OTUD7b and TAK1 in the nucleus, as well as to evaluate the expression levels of OTUD7b in NRPCs across different treatment groups. Cells seeded on coverslips were fixed using 4% paraformaldehyde for 15 min at room temperature. The cells were permeabilized using 0.1% Triton X-100 for 20 min, followed by blocking with 5% donkey serum at room temperature for 30 min. Cells on the coverslips were incubated overnight at 4 °C with a primary antibody mixture containing OTUD7b (1:200; 16605-1-AP, Proteintech) and α-actinin (1:200; ab9465, Abcam). Following primary antibody incubation, the cells were treated with fluorescently labeled secondary antibodies at 37 °C for 1 h. Finally, the nuclei were counterstained with DAPI.

When primary antibodies were raised in the same species, cellular immunofluorescence staining was conducted using a TSA kit (RC0086Plus-34R, Record Biological Technology Co. Ltd). The staining procedure was performed strictly according to the instructions provided by the reagent manufacturer. Following the fixation with 4% paraformaldehyde and permeabilization, the cells were incubated with 3% H_2O_2 at room temperature for 15 min in the dark to inhibit endogenous catalase activity. Cells were blocked with 5% bovine serum albumin (BSA) to reduce nonspecific binding, followed by overnight incubation with the primary antibody against OTUD7b (1:200; 16605-1-AP, Proteintech). Subsequently, the cells were incubated with horseradish peroxidase (HRP)-conjugated secondary antibody for 50 min, and OTUD7b fluorescence labeling was achieved with the appropriate TSA fluorescent dye reaction solution. After eluting the antibody, the fluorescence labeling protocol for TAK1 (1:300; 12330-2-AP, Proteintech) was performed by repeating the above-mentioned steps. Finally, nuclei were counterstained with DAPI. Fluorescence images were acquired from a confocal microscope, and blinded quantitative analysis was conducted using ImageJ software.

scRNA-seq processing

Heart tissues were harvested, and scRNA-seq was subsequently conducted in collaboration with LC-Bio Technologies (Hangzhou, China). Upon receiving the sequencing data, the Seurat package (Version 3.2.0) within the R software (version 4.2.1) was utilized to perform cross-sample normalization, data processing, and quality control. Low-quality cells were excluded, and the gene expression matrices were normalized using the NormalizeData function. Subsequently, 2000 highly variable features were identified using the FindVariableFeatures function to capture genes with significant cell-to-cell variation. Dimensionality reduction and cell clustering were performed using the RunPCA, FindNeighbors, and FindClusters functions. Additional dimensionality reduction was carried out using the RunUMAP and RunTSNE functions. Cell clusters were annotated by comparing their gene expression profiles with known cell type-specific markers, enabling the assignment of clustered cells to their respective cell types. Average expression levels were calculated, and the $\log_2$(|fold change|) between the target cell cluster and all other cells was used as the test statistic for subsequent analyses.

Transcriptome sequencing

Total RNA was extracted from the cardiac tissues of *Otud7b*$^{fl/fl}$-T2DM mice and *Otud7b* CKO-T2DM mice using TRIzol Reagent (9108, Takara, Tokyo, Japan), followed by transcriptome sequencing. RNA purity and concentration were assessed with the Agilent 2100 Bioanalyzer (Thermo Fisher Scientific, Waltham, USA) and the NanoDrop ND-1000 spectrophotometer (NanoDrop, Wilmington, USA). RNA quality was assessed by denaturing agarose gel electrophoresis, followed by the purification of mRNA using magnetic beads conjugated with oligo(dT) primers. Purified mRNA was fragmented into short pieces using the lysis buffer under controlled temperature conditions.

These cleaved RNA fragments were subsequently reverse-transcribed into cDNA using random hexamer primers. To complete the repair process, an A-tailing Mix and RNA Index Adapters were added, followed by incubation. Sequencing was conducted on the BGISEQ-500 platform (Beijing Genomics Institute, Shenzhen, China).

Clean reads were aligned to reference genes and the genome using Bowtie2 (v2.2.5) and HISAT2 (v2.0.4). Gene expression levels, measured as fragments per kilobase of transcript per million mapped reads (FPKM), were quantified by RSEM (v1.2.12). Differentially expressed genes (DEGs) were identified using the DESeq2 package in R, applying thresholds of $\log_2$(|fold change|) > 2 and an adjusted *P*-value < 0.05. Pathway enrichment analysis of DEGs was conducted by the Kyoto Encyclopedia of Genes and Genomes (KEGG) database (https://www.kegg.jp/), and potential transcription factors were predicted using the Enrichr platform (https://maayanlab.cloud/Enrichr/).

Real-time qPCR (RT-qPCR)

RNA was extracted from the mouse heart tissues and the cultured cells using TRIzol reagent (9108, Takara) according to the manufacturer's protocol. The cDNA was synthesized with the Hifair® III 1st Strand cDNA Synthesis Super Mix (11120ES60, YEASEN, Shanghai, China). The cDNA fragments were amplified using the SYBR Green Master Mix (11201ES60, YEASEN) on a

CFX96 System (Bio-Rad, Hercules, USA). All primers utilized in this study were purchased from Sangon Biotech (Shanghai, China) and are listed in Supplementary Table 1, with β-actin serving as the endogenous reference gene.

Cell culture

NRPCs were isolated from P0 Sprague Dawley (SD) neonatal rat hearts using a previously established protocol [10]. Following disinfection with 75% alcohol, the chest cavity was surgically opened to extract the heart, which was subsequently rinsed with phosphate-buffered saline (PBS). The ventricular tissue was sectioned into smaller fragments and subjected to enzymatic digestion in a digestion solution at 37 °C for 8 min with controlled agitation. The digestion solution was prepared by dissolving 0.16 g of trypsin (T8150, Solarbio, Beijing, China), 0.07 g of $NaHCO_3$ (A100865-0500, Sangon), 1.6 g of NaCl (A100865-0500, Sangon), 0.198 g of glucose (50997, Sangon), 0.059 g of KCl (A100395-0100, Sangon), and 0.4 g of HEPES (A600264-0050, Sangon) in 200 mL of double-distilled water (ddH_2O). The mixture was thoroughly shaken and subsequently filtered to ensure homogeneity. The supernatant containing blood cells was collected when it became pale, and the enzymatic digestion was terminated by adding the termination medium. The termination medium was prepared using Dulbecco's Modified Eagle's Medium (DMEM; 11965-092, Gibco, New York, USA) supplemented with 20% fetal bovine serum (FBS; 13011-8611, TianHang Biotechnology, Zhejiang, China).

Digestion was considered complete when the supernatant became nearly colorless and transparent, with minimal visible tissue fragments remaining. The digestion solution was centrifuged after every 2–3 rounds of collection. The pellet obtained following centrifugation was resuspended in DMEM with 10% FBS and cultured under adherent conditions in an incubator. After 1.5 h of incubation, the supernatant was collected and centrifuged. The obtained precipitate was resuspended in DMEM containing 10% FBS and cultured as NRPCs. Experiments were conducted after NRPCs achieved complete adherence and stability. The HG + PA group was treated with DMEM supplemented with 33 mM D-glucose and 100 μM palmitic acid at various time points. The 5.5 mM D-glucose group served as the control group in this study. As an osmotic control, a mannitol solution (33 mM total, 5.5 mM of glucose, and 27.5 mM of D-mannitol) was used to match the osmolarity of the HG condition.

The human embryonic kidney cell line (Hek293T) was provided by the Shanghai Cell Bank of the Chinese Academy of Sciences (Shanghai, China). The DMEM supplemented with 10% FBS was used to culture Hek293T cells. All types of cells were cultured in a humidified incubator at 37 °C with 5% CO_2.

Cytokine measurement by ELISA

The levels of TNF-α and IL-6 in the samples were quantified using ELISA kits (TNF-α: BMS607-3; IL-6: BMS603-2; Thermo Fisher Scientific, Waltham, MA, USA). All assays were performed strictly in accordance with the manufacturer's instructions. Briefly, samples, standards, and controls were added to the pre-coated plates, followed by incubation with biotin-conjugated detection antibody and streptavidin-HRP. Optical density was measured at 450 nm using a microplate reader, and cytokine concentrations were calculated from standard curves generated with the kit's recombinant protein standards.

Gene knockdown and overexpression

Small interfering RNA (siRNA) was transfected into NRPCs to achieve OTUD7b knockdown. The human OTUD7b siRNA was synthesized by GenePharma Co., Ltd. (Shanghai, China), with the sense as 5′-CCUCAGUGACUUUGAACAATT-3′ and the antisense as 5′-UUGUUCAAAGUCACUGAGGTT-3′. The negative control (NC) was transfected into NRPCs as a control group. Cells in optimal condition were cultured in 6 cm dishes until they reached the appropriate confluence. Following the manufacturer's protocol, the cells were transfected with 60 nM siRNA using jetPRIME® transfection reagent (101000046, Polyplus, Strasbourg, France). After 24 h of transfection, the cells were harvested for subsequent analysis.

The following plasmids were constructed by Unibio (Changsha, China): Flag-OTUD7b-WT (WT, wild type), Flag-OTUD7b-ΔUBA (ΔUBA, Δ41-841), Flag-OTUD7b-ΔOTU [ΔOTU, Δ (1-188 + 360-841)], Flag-OTUD7b-ΔZF (ΔZF, Δ1-797), Flag-OTUD7b-H358A, Flag-OTUD7b-C194A, HA-TAK1-WT, His-TAK1-WT, His-TAK1-K72R, His-TAK1-K346R, His-TAK1-K547R, Myc-Ub, Myc-Ub-K63 and Myc-Ub-K48. The plasmids listed above were selected based on the specific experimental objectives and transfected into Hek293T cells using jetPRIME® transfection reagent (101000046, Polyplus).

Cycloheximide (CHX) chase assay

The CHX chase assay was performed to examine the degradation kinetics of TAK1. NRPCs were transfected with TAK1 plasmids, siOTUD7b, or OTUD7b plasmids. After 24 h of transfection, cells were washed with PBS to remove the transfection reagent, and cycloheximide was added at a final concentration of 100 μM (C7698, Sigma-Aldrich). Subsequently, cell lysis buffer for Western blot and IP (P0013, Beyotime Biotechnology) was added at the indicated time points (0, 3, 6, and 9 h) following the addition of cycloheximide. The cells were then processed for Western blot analysis.

Liquid chromatography tandem mass spectrometry (LC-MS/MS) analysis

Anti-Flag antibody was added to the lysate samples from cardiomyocytes transfected with Flag-OTUD7b plasmids for immunoprecipitation (IP) experiments. IgG was used as a negative control to assess nonspecific binding. Then, the samples were processed and sent following the sample delivery protocol provided by PTM Bio Co., Ltd. (Hangzhou, China), where LC-MS analysis was performed. Finally, substrate proteins that could bind OTUD7b were identified based on their scores and protein quality.

Western blotting

Total protein extracts were prepared from mouse heart tissues and cultured cells with Cell & Tissue Protein Extraction Reagent (KC415, Kangcheng Bioengineering, Shanghai, China). Cytoplasmic and nuclear proteins were extracted with the Nuclear and Cytoplasmic Protein Extraction Kit (P0028, Beyotime Biotechnology) according to the manufacturer's protocol. Equal amounts of protein were loaded, separated by sodium dodecyl sulfate-polyacrylamide gel electrophoresis (SDS-PAGE), and subsequently transferred onto polyvinylidene difluoride (PVDF) membranes using the wet transfer method. The PVDF membranes were initially blocked with 5% skimmed milk at room temperature for 1 h and washed with TBS-Tween (TBST) buffer, followed by incubation with the primary antibodies overnight at 4 °C. The primary antibodies used in this study were OTUD7b (1:1000; 16605-1-AP, Proteintech), MYH (1:1000; sc-376157, Santa Cruz Biotechnology, Dallas, USA), p-JNK (1:1000; 9255, Cell Signaling Technology), JNK (1:1000; 9252, Cell Signaling Technology), p-p38 (1:1000; 4511, Cell Signaling Technology), p38 (1:1000; 14064-1-AP, Proteintech), p-c-Jun (1:1000; 3270, Cell Signaling Technology), c-Jun (1:1000; 9165, Cell Signaling Technology), p-ATF2 (Thr71, Thr53) (1:1000; 27934, Cell Signaling Technology), TAK1 (1:1000; 12330-2-AP, Proteintech), Lamin B (1:1000; 66095-1-Ig, Proteintech), and GAPDH (1:2000; 60004-1-Ig, Proteintech). The PVDF membranes that were previously incubated with the primary antibodies overnight were subsequently incubated with the HRP-conjugated secondary antibody at room temperature for 2 h. Protein bands were then visualized using an enhanced chemiluminescence (ECL) detection kit (Servicebio, Wuhan, China). Quantitative analysis of protein bands was performed by ImageJ software (National Institutes of Health, Bethesda, USA). GAPDH was used as the internal standard for total and cytoplasmic proteins, while Lamin B served as the internal standard for nuclear proteins.

Co-IP

For the Co-IP experiments involving heart tissues and NRPCs, fresh heart tissues and cells stimulated by HG + PA were harvested for protein extraction. For experiments involving Hek293T cells, the relevant plasmids were transfected according to the specific experimental objectives, followed by cell lysis to prepare samples for analysis. Cell lysis buffer for Western blot and IP (P0013, Beyotime Biotechnology), supplemented with an appropriate concentration of phenylmethanesulfonyl fluoride (PMSF) to inhibit protease activity, was used to extract total protein lysates. A portion of the protein lysates was reserved as input controls, while the remaining lysates were incubated with specific primary antibodies overnight at 4 °C. Subsequently, the antibody-protein complexes were captured with protein A/G agarose beads (P0025, Beyotime Biotechnology) through incubation at 4 °C for 6 h. Finally, the beads were washed thoroughly four times with PBS to remove non-specific binding, and then 2× protein loading buffer to elute the bound proteins and prepare the samples for subsequent analysis. The primary antibodies utilized in this experiment included Flag-tag antibody (20543-1-AP, Proteintech), HA-tag antibody (51064-2-AP, Proteintech), His-tag antibody (10001-0-AP, Proteintech), OTUD7b antibody (16605-1-AP, Proteintech), and rabbit IgG antibody (A7016, Beyotime Biotechnology).

Deubiquitination assay

Hek293T cells were transfected with plasmids containing various tags according to the specific experimental objectives. Before harvesting, the transfected cells were treated with 10 μM MG132 for 6 h to inhibit proteasomal degradation. Cells were subsequently lysed with cell lysis buffer for Western and IP (P0013, Beyotime Biotechnology), followed by centrifugation at 12,000 rpm for 10 min at 4 °C to remove cellular debris. Immunoprecipitation was performed using Flag-tag antibody (20543-1-AP, Proteintech), HA-tag antibody (51064-2-AP, Proteintech), or His-tag antibody (10001-0-AP, Proteintech) to specifically capture the target proteins. The ubiquitination status of the immunoprecipitated proteins was then assessed by immunoblotting.

Statistical analysis

All data were derived from at least three independent experiments and were presented as the mean ± standard error of the mean (SEM). The exact sample size (*n*) for each experiment is specific, with "*n*" referring to the number of biological replicates rather than technical replicates. An unpaired *t*-test was employed for comparisons between two groups, while a one-way analysis of variance (ANOVA) followed by the Bonferroni *post hoc* test was applied for comparisons among multiple groups. Statistical analyses and graph generation were performed with GraphPad Prism version 8.01 (GraphPad Software, San Diego, USA). A *P*-value of less than 0.05 was considered statistically significant.

RESULTS

Cardiomyocyte-derived OTUD7b is markedly upregulated in diabetic hearts

To investigate the potential involvement of OTUD7b in the pathogenesis of DCM, we first assessed its expression in mice with T1DM or T2DM. As shown in Fig. 1a, b, the mRNA levels of *Otud7b* were significantly increased in the cardiac tissues from T2DM and T1DM mice. Immunoblot analysis confirmed a parallel increase in OTUD7b protein levels in diabetic hearts compared to the control group (Fig. 1c–f). To map its cellular origin, we re-analyzed our previously generated single-cell RNA sequencing (scRNA-seq) dataset from diabetic mouse hearts [5]. Among the five major populations, including cardiomyocytes (CMs), fibroblasts (FBs), endothelial cells (ECs), smooth muscle cells (SMCs), and immune cells (ICs), the mRNA level of *Otud7b* was overwhelmingly enriched in CMs (Fig. 1g, h). Immunoblotting validated that OTUD7b expression in neonatal rat primary cardiomyocytes (NRPCs) is higher than in neonatal rat primary fibroblasts (NRPFs), myeloid-derived macrophages (MDMs), or mouse cardiac microvascular endothelial cells (MCMECs) (Fig. 1i). In cultured NRPCs, high glucose and palmitic acid (HG + PA) stimulation elevated OTUD7b protein expression in a time-dependent manner (Fig. 1j, k). Osmotic control experiments using a solution containing 5.5 mM glucose plus 27.5 mM D-mannitol were performed and showed similar results (Fig. S1a, b). The cellular origin of OTUD7b was further evaluated in diabetic mouse hearts using double-immunofluorescence staining. As shown in Fig. 1l, m, OTUD7b upregulation occurred predominantly in α-actinin^{+} cardiomyocytes, not in vimentin^{+} fibroblasts. Collectively, we identified that cardiomyocyte OTUD7b expression is markedly elevated in diabetic hearts.

OTUD7b mediates HG + PA-induced cardiomyocyte hypertrophy in vitro

To understand the role of OTUD7b in cardiomyocyte hypertrophy under diabetic conditions, we modulated its expression in HG + PA-challenged NRPCs. Morphometric analysis showed that HG + PA stimulation led to an increase in cardiomyocyte area, which was significantly alleviated upon transfection with siRNA targeting OTUD7b (siOTUD7b; Fig. 2a). Immunoblotting confirmed efficient knockdown of OTUD7b protein by siOTUD7b reversed the HG + PA-induced upregulation of the hypertrophic marker myosin heavy chain (MYH) in NRPCs (Fig. 2b). Conversely, overexpression of OTUD7b via transfection of OTUD7b plasmid (OTUD7b^{oe}) amplified HG + PA-induced hypertrophic phenotypes, including increased cell size and elevated MYH expression (Fig. 2c, d). In addition, there was no significant difference in cell area between the osmotic control group and the 5.5 mM glucose group Fig. S1c. These data indicate OTUD7b as a pathological factor in cardiomyocyte hypertrophy under diabetic conditions.

Cardiomyocyte-specific deletion of OTUD7b alleviates cardiac dysfunction and remodeling in T2DM mice

To identify the in vivo contribution of OTUD7b to DCM, we generated cardiomyocyte-specific OTUD7b knockout mice (*Otud7b* CKO) using a tamoxifen (TAM)-inducible *Myh6*-Cre system (Fig. S2a, b). TAM injection for 5 continuous days induced a significant decrease in cardiomyocyte OTUD7b level in *Otud7b* CKO mice (Figs. 3a and S2c, d). After TAM injection, *Otud7b* CKO mice and littermate *Otud7b-flox (Otud7b$^{fl/fl}$)* mice were subjected to a T2DM protocol combining low-dose streptozotocin (STZ; 35 mg/kg) and a high-fat diet (HFD) for 16 weeks (Fig. 3a). We assessed the levels of blood glucose and body weight and found no difference in T2DM mice with or without *Otud7b* knockout (Fig. 3b, c). Subsequently, a non-invasive echocardiography examination was performed on the 24-week-old mice. Compared with age-matched *Otud7b$^{fl/fl}$* mice, *Otud7b* CKO mice exhibited alleviated cardiac systolic dysfunction in diabetic mice, characterized by increased values of ejection fraction (EF%) and fractional shortening (FS%), and decreased left ventricular internal diameter (LVIDd) and interventricular septal thickness (IVSD) (Fig. 3d–f and Supplementary Table 2). Gross heart size was reduced in diabetic *Otud7b* CKO mice (Fig. 3g), and histological analysis using H&E and WGA staining confirmed that *Otud7b* CKO inhibited T2DM-induced cardiac hypertrophy (Fig. 3h–j). Western blot assay confirmed *Otud7b* CKO decreased MYH expression in diabetic hearts (Fig. 3k, l). In addition, examinations on cardiac fibrosis, including RT-qPCR analysis for *Col1a1* and *Tgfb1* mRNA levels and Masson's trichrome/Sirius red staining, showed that *Otud7b* CKO significantly limited interstitial fibrosis and collagen deposition in diabetic heart tissues (Figs. 3m–o and S3a, b). These findings

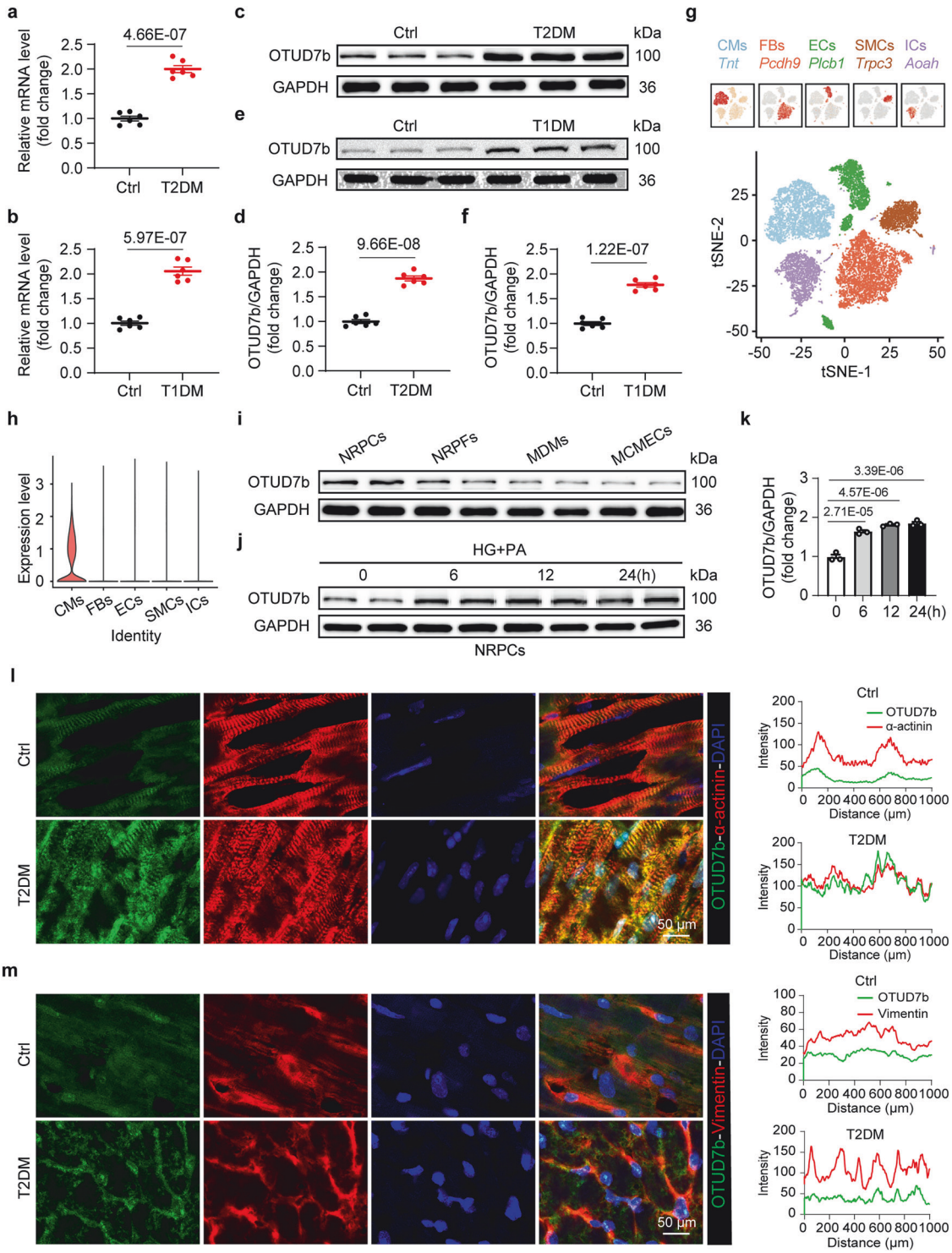

Fig. 1 Cardiomyocyte-derived OTUD7b is markedly upregulated in diabetic hearts. a, **b** The mRNA levels of *Otud7b* in the heart tissues from T2DM and T1DM mice. **c**–**f** Representative immunoblot and densitometric analysis of OTUD7b in heart tissues from T2DM and T1DM mice. **g** The t-SNE plot identified five main cell types, including cardiomyocytes (CMs), fibroblasts (FBs), endothelial cells (ECs), smooth muscle cells (SMCs), and immune cells (ICs) in scRNA-seq analysis. **h** A violin plot showing the expression pattern of *Otud7b* across these cell clusters. **i** Western blot analysis of OTUD7b protein expression in different cell types, including neonatal rat primary cardiomyocytes (NRPCs), neonatal rat primary fibroblasts (NRPFs), myeloid-derived macrophages (MDMs), and mouse cardiac microvascular endothelial cells (MCMECs). **j**, **k** Time-course of OTUD7b protein expression in NRPCs exposed to high glucose (HG; 33 mM) and palmitic acid (PA; 100 μM) for indicated times (0, 6, 12, and 24 h). **l** Representative images of immunofluorescence staining and fluorescence-intensity quantification of OTUD7b (green), α-actinin (red) and DAPI (blue) in heart tissues from T2DM mice. **m** Immunofluorescence staining and fluorescence-intensity quantification of OTUD7b (green), Vimentin (red) and DAPI (blue) in heart tissues from T2DM mice. For **l**, **m**, scale bar = 50 μm. Data are shown as mean ± SEM; **a**–**f**: $n = 6$; **g**–**k**: $n = 3$. For **a**, **b**, **d**, **f**, *P* values were determined by Student *t* test; For **k**, *P* values were determined by one-way ANOVA followed by Tukey *post hoc* tests. *P* values indicated.

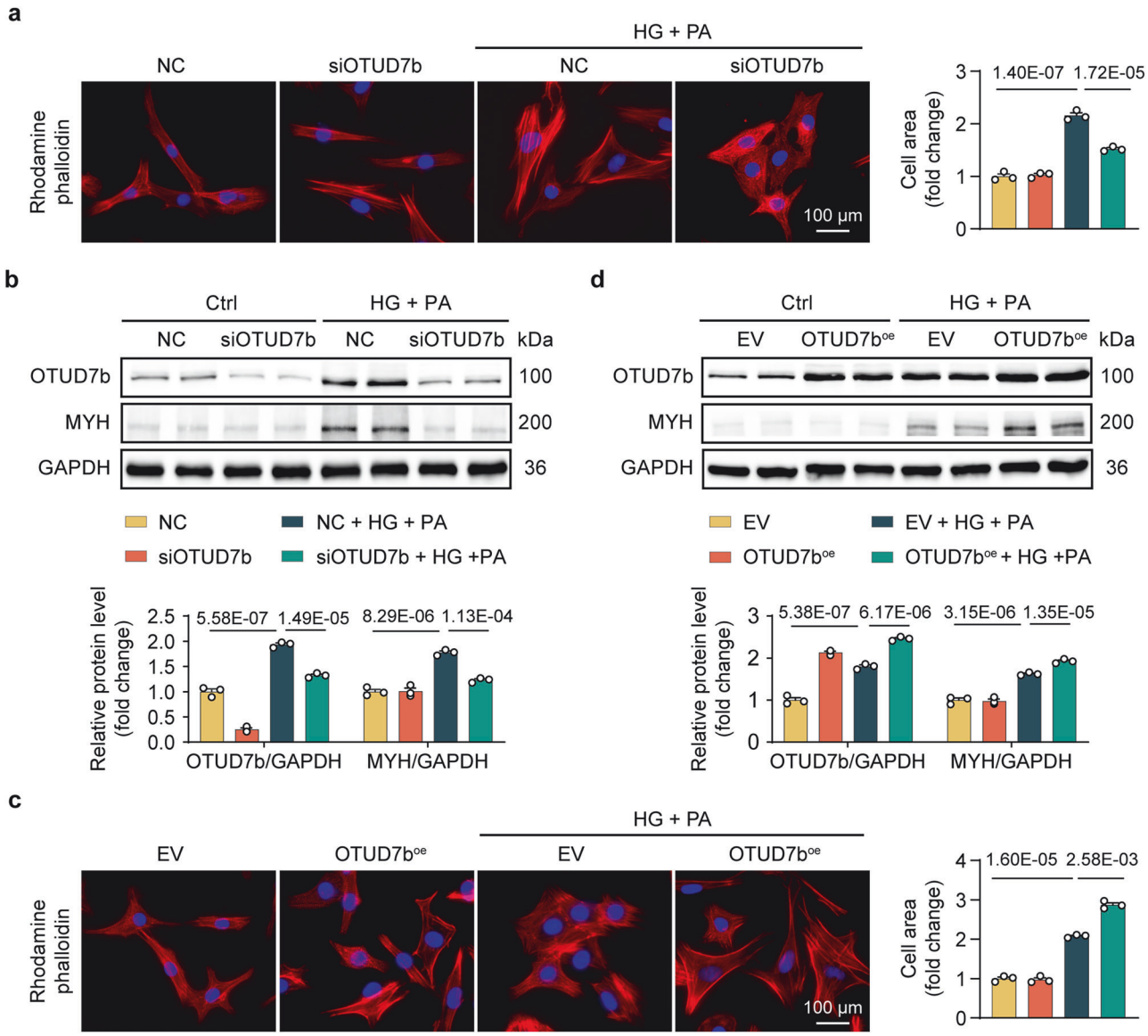

Fig. 2 OTUD7b exacerbates high glucose (HG) and palmitic acid (PA) induced cardiomyocyte hypertrophy in vitro. a Neonatal rat primary cardiomyocytes (NRPCs) transfected with siRNA targeting OTUD7b (siOTUD7b) or scrambled negative control (NC), and subsequently stimulated with HG (33 mM) and PA (100 μM). Representative images of rhodamine phalloidin staining and quantification of cell area were shown. **b** Western blot analysis and densitometric quantification of OTUD7b and MYH in NRPCs treated as indicated. **c** NRPCs transfected with OTUD7b plasmids (OTUD7b^{oe}), or empty vector (EV), were challenged with HG and PA. Representative images of rhodamine phalloidin staining and quantification of cell area. **d** Representative immunoblot and densitometric analysis of OTUD7b and MYH. For **a**, **c**, scale bar = 100 μm. Data are shown as mean ± SEM; $n = 3$. *P* values were determined by one-way ANOVA followed by Tukey *post hoc* tests. *P* values indicated.

suggest that cardiomyocyte-specific deletion of OTUD7b protects against DCM in T2DM mice.

Otud7b CKO prevents DCM in T1DM mice

To determine whether the pathological role of OTUD7b extends to T1DM, we subjected *Otud7b* CKO and *Otud7b*$^{fl/fl}$ mice to a high-dose STZ-induced T1DM protocol (Fig. 4a). As expected, diabetic mice displayed hyperglycemia and weight loss during 16 weeks of monitoring, which were also unaffected by OTUD7b deletion (Fig. 4b, c). Echocardiographic evaluation revealed that *Otud7b* CKO mice exhibited preserved cardiac systolic function compared to diabetic controls (Fig. 4d–f and Supplementary Table 3). Gross heart morphology and histological assessment revealed reduced heart size and smaller cardiomyocyte cross-sectional area in *Otud7b* CKO T1DM mice than in *Otud7b*$^{fl/fl}$ mice (Fig. 4g–j). The expression of hypertrophic protein followed a similar trend (Fig. 4k, l). Likewise, OTUD7b deficiency attenuated fibrotic gene expression (*Col1a1* and *Tgfb1*) and collagen deposition in diabetic hearts (Figs. 4m–o and S4a, b). These data confirm that cardiomyocyte-specific ablation of OTUD7b also confers robust protection against T1DM-induced cardiomyopathy.

Identification of TAK1 as a potential substrate of OTUD7b

To explore the potential substrate of OTUD7b that regulates DCM, we conducted a comprehensive analysis combining ubiquitinome and interactome assays in cardiomyocytes (Fig. 5a). In total, the interactome assay identified 853 OTUD7b-binding proteins, of which five proteins were deubiquitinated in OTUD7b-

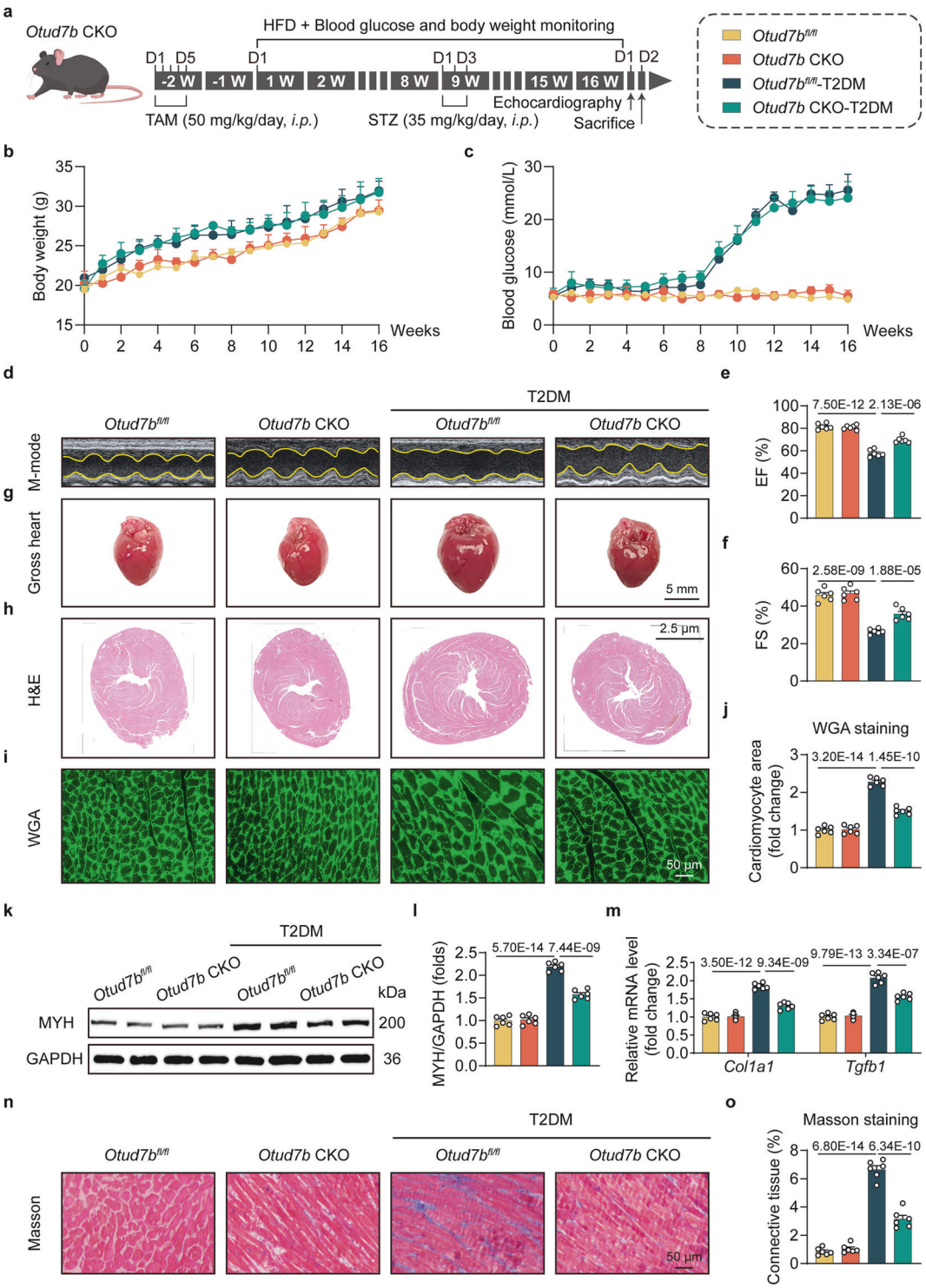

Fig. 3 Cardiomyocyte-specific deletion of OTUD7b alleviates cardiac dysfunction and remodeling in T2DM mice. a Schematic representation of the experimental design. Cardiomyocyte-specific OTUD7b knockout mice (*Otud7b* CKO) were generated using a tamoxifen (TAM)-inducible Myh6-Cre system and induced by 5 consecutive days of TAM administration. *Otud7b*$^{fl/fl}$ and *Otud7b* CKO mice were induced to T2DM by low-dose streptozotocin (STZ, 35 mg/kg) administration for 3 consecutive days, combined with high-fat diet (HFD) feeding for 16 weeks. After 16 weeks, the cardiac function of the mice was evaluated, and blood samples along with heart tissues were harvested. **b**, **c** Body weight and blood glucose levels of mice in the indicated groups. **d** Representative M-mode echocardiographic images of the indicated groups. **e**, **f** Values of ejection fraction (EF%) and fractional shortening (FS %) by echocardiography. **g** Representative images of the whole heart. **h** Representative images of H&E staining of transverse heart sections. **i**, **j** Wheat germ agglutinin (WGA) staining and quantification of cardiomyocyte area in heart tissues. **k**, **l** Western blot analysis and densitometric quantification of MYH in heart tissues. **m** The mRNA levels of fibrotic genes (*Col1a1* and *Tgfb1*) were quantified by RT-qPCR in heart tissues. **n**, **o** Representative images and quantification of Masson's Trichrome staining in heart tissues. For **g**, scale bar = 5 mm; For **h**, scale bar = 2.5 μm; For **i**, **n**, scale bar = 50 μm. Data are shown as mean ± SEM; $n = 6$. *P* values were determined by one-way ANOVA followed by Tukey *post hoc* tests. *P* values indicated.

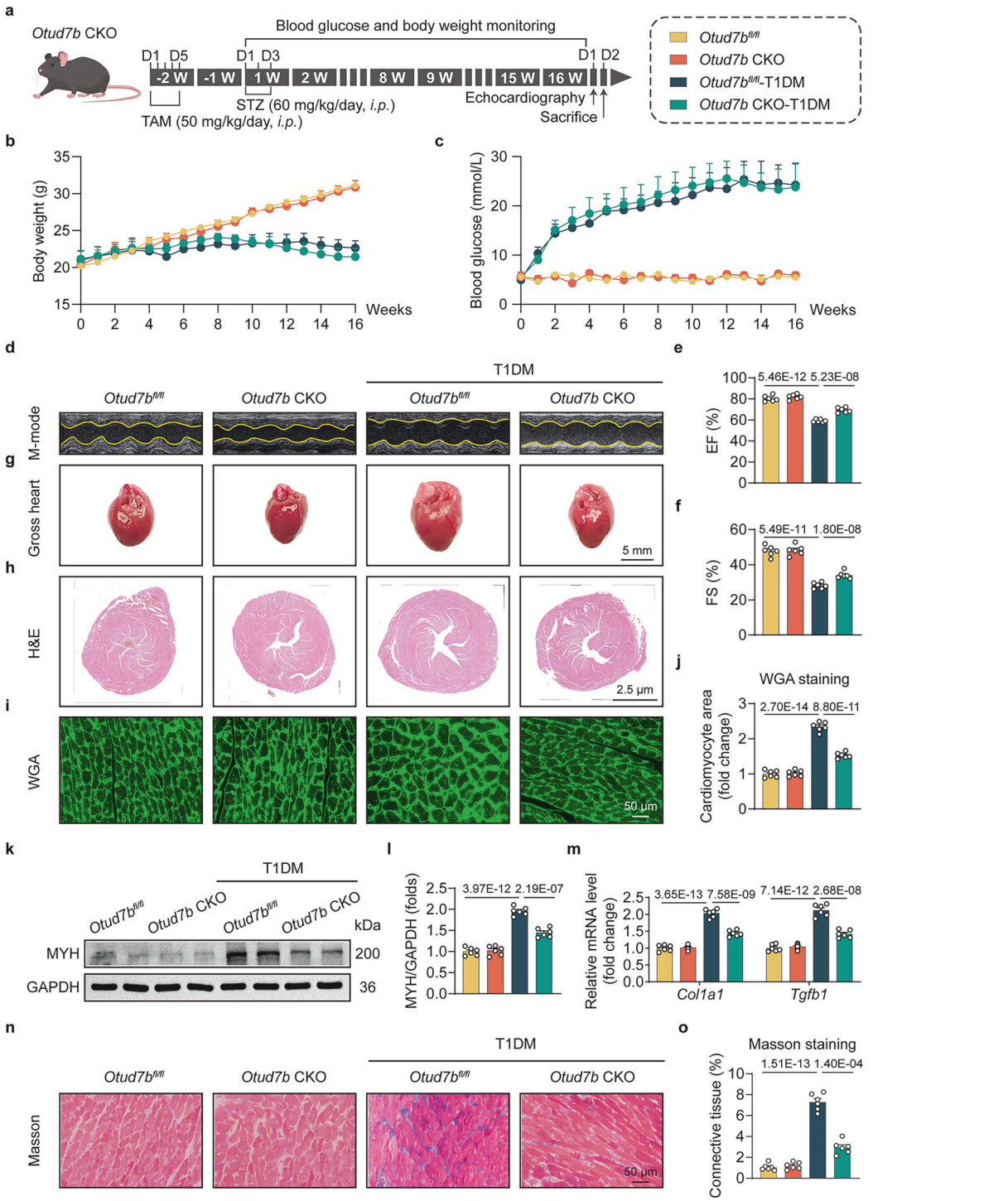

Fig. 4 Cardiomyocyte-specific OTUD7b knockout prevents DCM in T1DM mice. a Schematic of the experimental design. Cardiomyocyte-specific OTUD7b knockout mice (*Otud7b* CKO) were generated using a tamoxifen (TAM)-inducible Myh6-Cre system and induced by 5 consecutive days of TAM administration. *Otud7b*$^{fl/fl}$ and *Otud7b* CKO mice were induced to T1DM by high-dose streptozotocin (STZ, 60 mg/kg) injection for 3 consecutive days. Sixteen weeks later, cardiac function was assessed, and blood and heart tissue samples were collected. **b**, **c** Body weight and blood glucose levels were monitored for 16 weeks. **d** Representative M-mode echocardiographic images in all groups of mice. **e**, **f** Values of ejection fraction (EF%) and fractional shortening (FS%). **g** Representative images of the whole heart in all groups of mice. **h** Representative H&E staining images of heart sections. **i**, **j** Representative images and quantification of wheat germ agglutinin (WGA) staining of heart tissues. **k**, **l** Western blot analysis and quantification of MYH in heart tissues. **m** The mRNA levels of *Col1a1* and *Tgfb1* in heart tissues. **n**, **o** Representative images and quantification of Masson's Trichrome staining of heart tissues. For **g**, scale bar = 5 mm; For **h**, scale bar = 2.5 μm; For **i**, **n**, scale bar = 50 μm. Data are shown as mean ± SEM; $n = 6$. *P* values were determined by one-way ANOVA followed by Tukey *post hoc* tests. *P* values indicated.

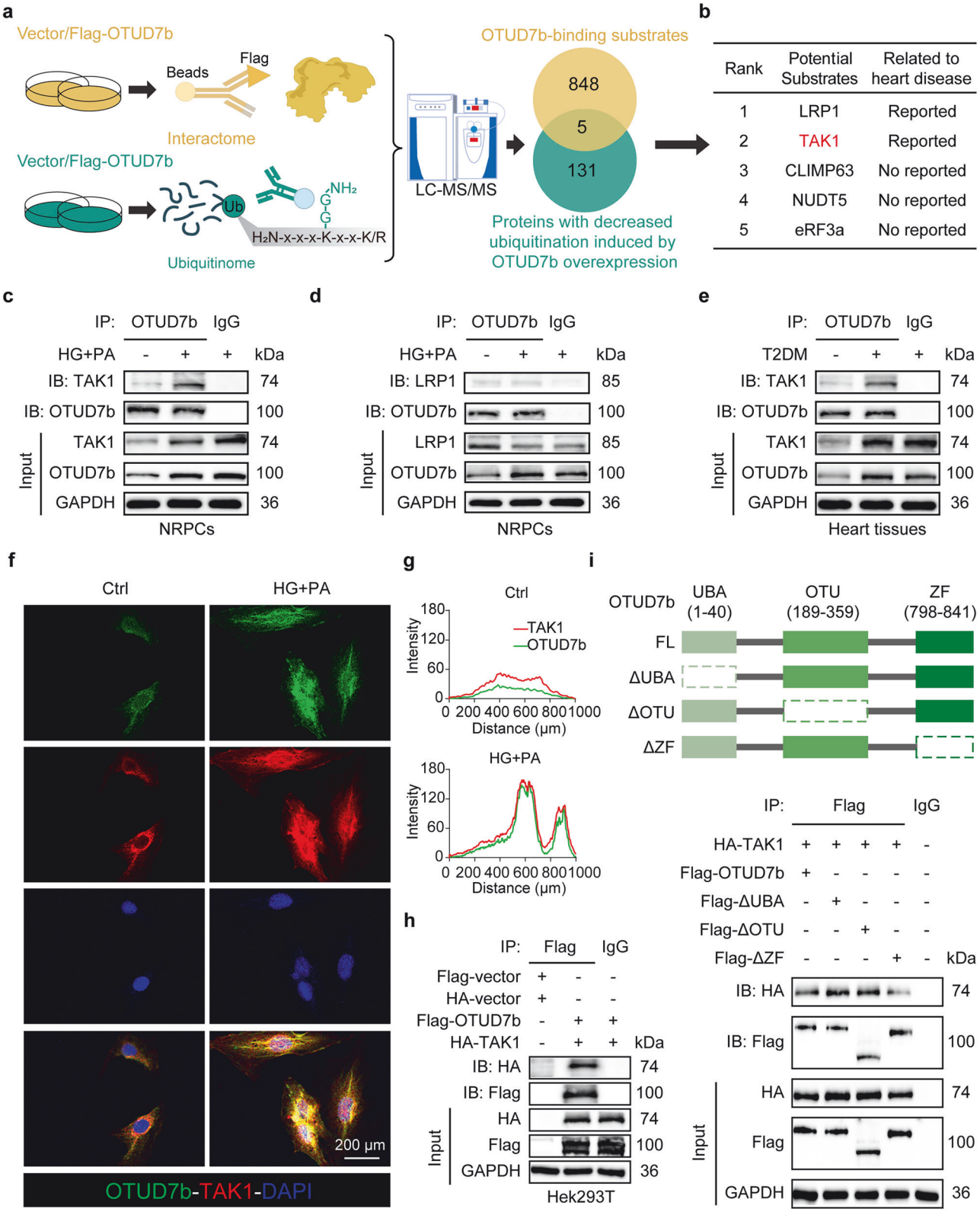

Fig. 5 Identification of TAK1 as a potential substrate of OTUD7b. a Schematic of a comprehensive analysis combining ubiquitinome and interactome assays for OTUD7b substrate screening. **b** Table for the five candidate substrates of OTUD7b that were screened. **c** Co-immunoprecipitation (Co-IP) of the interaction between OTUD7b and TAK1 in high glucose (HG; 33 mM) + palmitic acid (PA; 100 μM)-treated neonatal rat primary cardiomyocytes (NRPCs). **d** Co-IP of the interaction between OTUD7b and LRP1 in NRPCs treated as indicated. **e** Co-IP of the interaction between OTUD7b and TAK1 in heart tissues from T2DM mice. **f**, **g** Representative immunofluorescence images and intensity quantification of OTUD7b (green) and TAK1 (red) in NRPCs challenged with HG and PA. **h** Co-IP analysis of OTUD7b with TAK1 in Hek293T cells co-transfected with Flag-OTUD7b and HA-TAK1 plasmids. **i** Schematic diagram of truncated mutants of OTUD7b (top) and Co-IP analysis of TAK1 with either wild-type OTUD7b or OTUD7b mutants (bottom). For **f**, scale bar = 200 μm. $n = 3$.

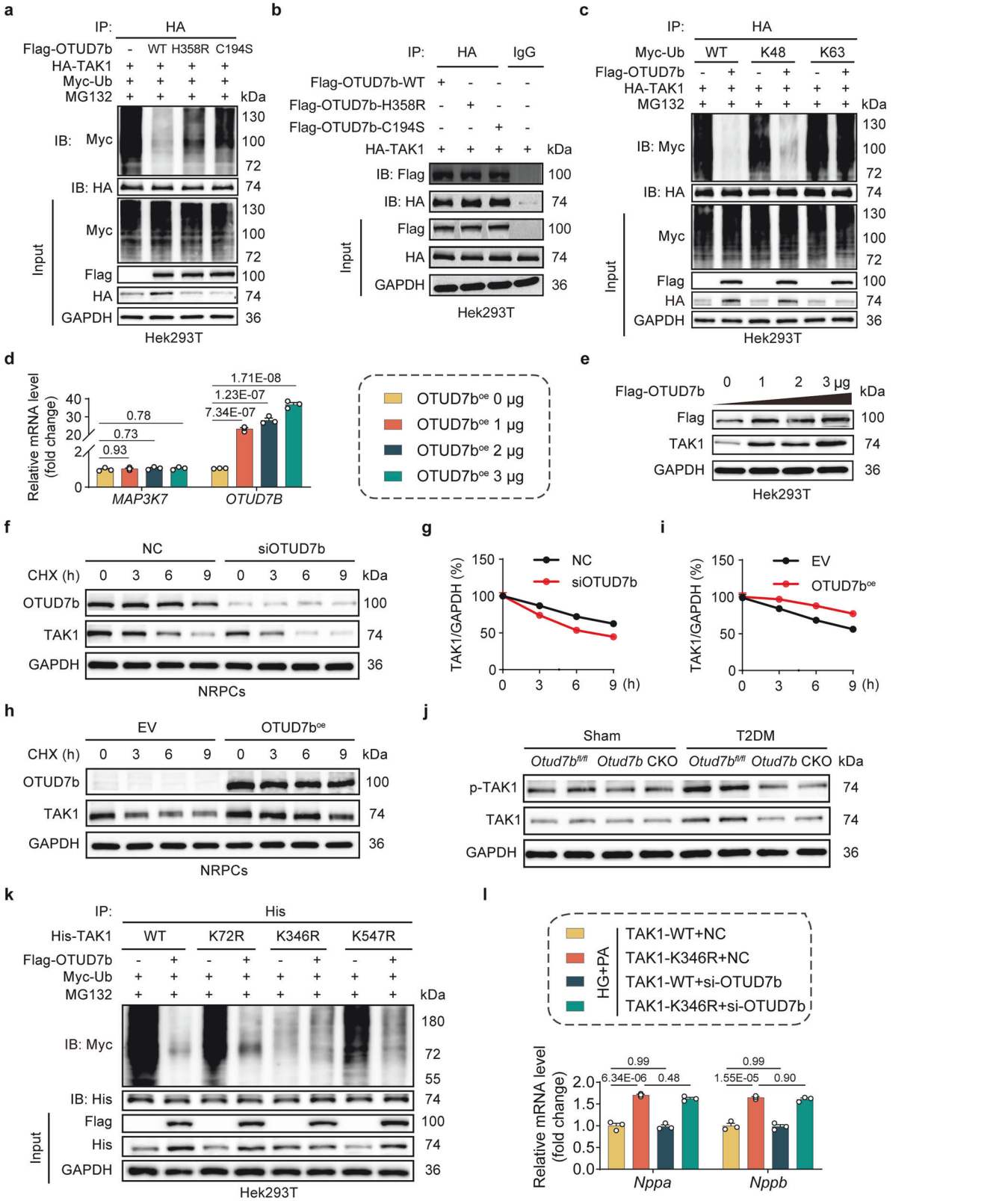

overexpressing cardiomyocytes. Among these five, only LRP1 [26] and TAK1 [27] have been reported to participate in cardiac diseases (Fig. 5b). We then examined the endogenous interaction between OTUD7b and both candidates in NRPCs. Strikingly, although both proteins bound OTUD7b, only the TAK1-OTUD7b interaction was significantly enhanced under HG + PA stress, suggesting its specific relevance to DCM progression (Figs. 5c, d and S5a, b). The peptide sequence map of TAK1 was shown in Fig. S5c. We further confirmed the interaction of TAK1-OTUD7b in diabetic heart tissues (Fig. 5e). Immunofluorescence double

Fig. 6 OTUD7b deubiquitinates and stabilizes TAK1 to promote TAK1 phosphorylation via its active site C194 and H358. a Hek293T cells were co-transfected with Myc-ubiquitin (Ub), HA-TAK1, and either Flag-OTUD7B-WT, Flag-OTUD7B-H358R, or Flag-OTUD7B-C194S plasmids, followed by treatment with 10 μM MG132 for 6 h. Ubiquitinated TAK1 was detected via immunoblotting. **b** Co-immunoprecipitation (Co-IP) of the interaction between OTUD7b and TAK1 in Hek293T cells treated as indicated. **c** Co-IP assay demonstrated the ubiquitination of TAK1 by K48-Ub or K63-Ub in Hek293T cells. **d** The mRNA levels of *MAP3K7* (the encoding gene of TAK1) and *OTUD7B* were quantified by RT-qPCR in Hek293T cells transfected with Flag-OTUD7b plasmids at indicated dose (1, 2, and 3 μg). **e** Western blot analysis of TAK1 in Hek293T cells treated as indicated. **f**, **g** Neonatal rat primary cardiomyocytes (NRPCs) transfected with TAK1 plasmids and siRNA targeting OTUD7b (siOTUD7b) or scrambled negative control (NC), followed by treatment with 100 μM cycloheximide (CHX) for 0, 3, 6 and 9 h. Western blot analysis and quantification of OTUD7b and TAK1. **h**, **i** Western blot analysis and quantification of OTUD7b and TAK1 in NRPCs co-transfected with OTUD7b plasmids ($OTUD7b^{oe}$) or Empty Vector (EV), followed by CHX treatment for 0, 3, 6 and 9 h. **j** Western blot analysis of p-TAK1 and TAK1 in heart tissues from sham and T2DM mice in both $Otud7b^{fl/fl}$ and *Otud7b* CKO groups. **k** Co-IP assay was performed in Hek293T cells co-transfected with Myc-Ub, Flag-OTUD7B, and either His-TAK1 (WT) or TAK1 mutants (K72R, K346R, or K547R) plasmids. Ubiquitinated TAK1 was detected by immunoblotting. **l** NRPCs were transfected with His-TAK1-WT and His-TAK1-K346R plasmids under OTUD7b silencing (siOTUD7b) conditions, then the NRPCs were exposed to high glucose (HG; 33 mM) and palmitic acid (PA; 100 μM). The mRNA levels of *Nppa* and *Nppb* were detected. Data are shown as mean ± SEM; **a**–**h**, **k** and **l**: $n = 3$; **j**: $n = 6$. *P* values were determined by one-way ANOVA followed by Tukey *post hoc* tests. *P* values indicated.

staining revealed robust intracellular co-localization of these two proteins in NRPCs exposed to HG + PA (Fig. 5f, g). Next, we co-transfected Flag-tagged OTUD7b and HA-tagged TAK1 in Hek293T tool cells, and verified the exogenous interaction of TAK1-OTUD7b by co-immunoprecipitation(Fig. 5h). To map the critical binding interface, we generated a series of truncated mutants of OTUD7b. Our results showed that TAK1 failed to bind to the mutant lacking the ZF domain (798-841 aa), suggesting the ZF domain is responsible for TAK1 recognition (Fig. 5i).

OTUD7b deubiquitinates TAK1 at the K346 site and then stabilizes it

As OTUD7b binds to TAK1, we then examined the influence of the deubiquitinating activity of OTUD7b on TAK1. We treated cells with MG132 to prevent proteasomal degradation of TAK1 and observed that Flag-OTUD7b overexpression decreased the level of TAK1 ubiquitination in Hek293T cells (Fig. 6a). In contrast, OTUD7b deficiency increased TAK1 ubiquitination in both diabetic heart tissues and HG + PA-induced cardiomyocytes (Fig. S6a, b). Catalytically inactive OTUD7b mutants (C194S or H358R) failed to remove ubiquitin molecules from TAK1 (Fig. 6a). We also found these OTUD7b mutants did not affect the OTUD7b-TAK1 interaction in Hek293T cells (Fig. 6b). These data indicate OTUD7b-mediated TAK1 deubiquitination depends on its DUB enzymatic activity. Further, we co-transfected K48- or K63-mutated ubiquitin plasmids and TAK1 plasmid in Hek293T cells with or without OTUD7b, and found that OTUD7b efficiently removed K48-linked ubiquitin chain from TAK1 (Fig. 6c). Since K48-linked polyubiquitination mediates proteasomal degradation of substrate [28], we next assessed TAK1 stability. OTUD7b overexpression did not change the mRNA level of *Map3k7* (the gene encoding TAK1), but significantly upregulated TAK1 protein level in Hek293T cells (Figs. 6d, e and S6c). Treatment with cycloheximide (a de novo protein synthesis inhibitor) showed TAK1 degradation rate was accelerated in siOTUD7b-transfected NRPCs, but slowed in Flag-OTUD7b-overexpressing NRPCs (Fig. 6f-i). We further examined whether OTUD7b-mediated TAK1 is accompanied by increased TAK1 activation. T2DM induced the upregulation of both TAK1 and p-TAK1 in heart tissues, and these increases were attenuated in *Otud7b* CKO mouse heart tissues (Figs. 6j and S6d). Similarly, OTUD7b knockdown reduced both TAK1 and p-TAK1 levels in HG + PA-challenged NRPCs, while OTUD7b overexpression exacerbated these changes (Fig. S6e). These findings indicate that OTUD7b increases TAK1 activation by deubiquitinating TAK1 and enhancing its protein stability in cardiomyocytes.

Three lysine (K) residues in TAK1 (K72, K346, and K547) have been identified as potential sites for K48-linked polyubiquitination (Supplementary Table 4) [29–32]; we therefore selected these residues as candidates to test for OTUD7b-mediated deubiquitination. We constructed TAK1 site-mutant plasmids (K72R, K346R, and K547R). Among these, the K346R mutant abolished OTUD7b-mediated deubiquitination (Fig. 6k). Importantly, Co-IP analysis confirmed that the K346R mutation did not disrupt the interaction between TAK1 and OTUD7b (Fig. S7a). Moreover, TAK1-K346R failed to promote TAK1 degradation (Fig. S7b). These results confirm that K346 of TAK1 is the specific site for OTUD7b-mediated deubiquitination rather than an interface for protein-protein binding. We further examined whether OTUD7b-mediated cardiomyocyte hypertrophy depends on TAK1 deubiquitination at the K346 site. As shown in Fig. 6l, TAK1 K346R mutation exacerbated HG + PA-induced hypertrophic gene transcription, and siOTUD7b failed to inhibit the increases in hypertrophy genes in NRPCs with TAK1 K346R mutant. Osmotic control did not affect the transcription of the hypertrophic gene in NRPCs (Fig. S7c). These findings clarify OTUD7b targets K48-linked ubiquitination of TAK1 at the K346 site to regulate its stability.

OTUD7b-TAK1 axis activates MAPKs pathways and drives apoptosis and inflammation in cardiomyocytes

To further elucidate the molecular mechanisms by which the OTUD7b-TAK1 axis mediates cardiomyocyte injury, we performed bulk RNA-seq on cardiac tissues from diabetic *Otud7b* CKO mice and $Otud7b^{fl/fl}$ mice. Principal component analysis (PCA) demonstrated a clear separation between these two groups, indicating that transcriptomic alterations were induced by OTUD7b deletion in diabetic hearts (Fig. 7a). Analysis of DEGs identified 199 DEGs, comprising 155 downregulated genes and 44 upregulated genes in the *Otud7b* CKO diabetic group compared to the $Otud7b^{fl/fl}$ diabetic group (Fig. S8a). Gene Ontology (GO) enrichment and Gene Set Enrichment Analysis (GSEA) showed these DEGs were enriched in processes related to extrinsic apoptosis and inflammatory responses (Figs. 7b, c and S8b). Subsequent analysis of the expression profile of apoptosis- and inflammation-related genes further confirmed this involvement (Fig. 7d). Notably, KEGG pathway analysis revealed these DEGs were predominantly enriched in several signaling pathways, including MAPK pathway and cytokine/chemokine pathway (Fig. 7e), which are also well known to be major downstream pathway of TAK1 and mediate apoptosis and inflammatory reactions in cardiomyocytes [33, 34].

We then validated the involvement of the MAPK pathway in the OTUD7b-TAK1 axis. First, immunoblotting showed that the phosphorylation of MAPK components, including p-JNK, p-p38, and p-c-Jun, was significantly inhibited by OTUD7b deletion in the diabetic heart tissues (Figs. 7f and S9a). In vitro, our results showed that HG + PA-induced activation of the MAPK pathway was significantly suppressed in the OTUD7b knockdown NRPCs, while exacerbated by OTUD7b overexpression (Fig. S9b–e). Consistent with the inhibition of the MAPK pathway, OTUD7b knockout reduced the mRNA levels of inflammatory factors and chemokines, such as *Tnfa*, *Il6*, *Cxcl10*, and *Ccl22*, protein levels of

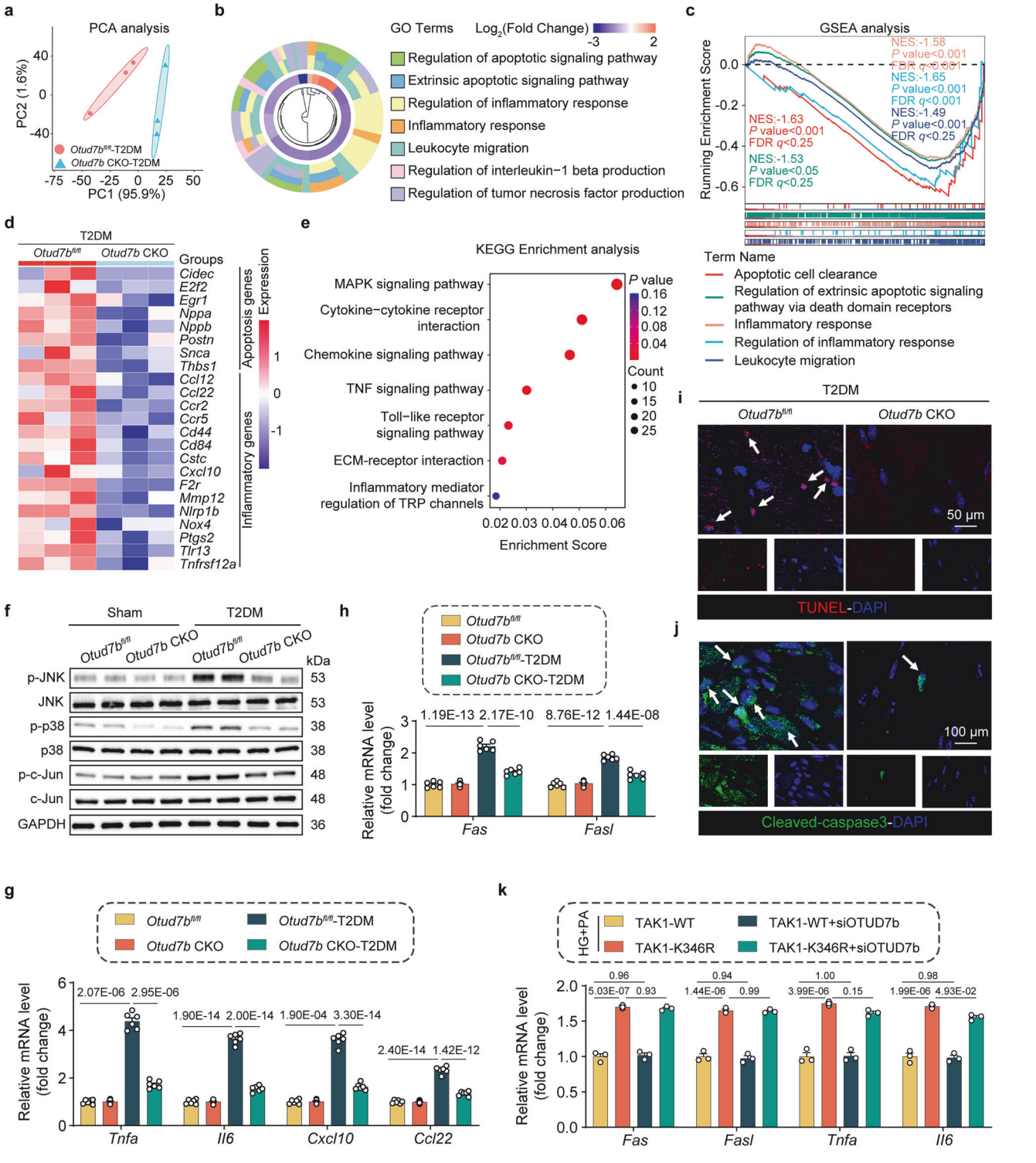

TNF-α and IL-6, and CD68^{+} macrophage infiltration in diabetic heart tissues (Figs. 7g and S9f–h). Next, we found that the mRNA levels of *Fas* and *Fasl*, and the activity of caspase 8 were significantly decreased in diabetic hearts from *Otud7b* CKO mice compared to *Otud7b*$^{fl/fl}$ mice (Figs. 7h and S10a). Similarly, the TUNEL^{+} and cleaved-caspase 3^{+} cells were markedly decreased in OTUD7b-deficient diabetic hearts (Figs. 7i, j and S10b, c), suggesting that loss of OTUD7b mitigates Fas/Fasl/caspase 8-mediated extrinsic apoptosis in diabetic cardiomyocytes.

Subsequently, we explored whether OTUD7b regulates apoptosis and inflammation via deubiquitinating TAK1 in cardiomyocytes. As shown in Figs. 7k and S10d, the TAK1 K346R mutant further enhanced the induction of apoptotic and inflammatory genes (*Fas*, *Fasl*, *Tnfa*, and *Il6*) compared to wild-type TAK1 in HG + PA-challenged NRPCs, and siOTUD7b failed to reverse this gene overexpression mediated by TAK1 K346R. Together, these findings confirm that the OTUD7b-TAK1 axis activates the MAPK pathway and then drives apoptosis and inflammation in cardiomyocytes.

Fig. 7 OTUD7b-TAK1 axis activates MAPKs pathways and drives apoptosis and inflammation in cardiomyocytes. a Bulk RNA-sequencing was performed in hearts tissues from T2DM mice in *Otud7b*$^{fl/fl}$ and *Otud7b* CKO groups. Principal-component analysis (PCA) visualized the transcriptomic separation of the two groups. **b** Gene Ontology (GO) enrichment analysis related pathway and biological process of differentially expressed genes (DEGs) between two groups. **c** Gene Set Enrichment Analysis (GSEA) related to extrinsic apoptosis and inflammatory response. *P* value indicates the statistical significance of the enrichment. FDR *q* value represents the *P* value adjusted for multiple testing. Results are considered significant at *P* value < 0.05 and FDR *q* value < 0.25. **d** Heat map of the apoptosis and inflammatory-related DEGs between the two groups. **e** Kyoto encyclopedia of genes and genomes (KEGG) enrichment analysis of DEGs. **f** Western blot analysis of MAPK components (p-JNK, JNK, p-p38, p38, p-c-Jun, and c-Jun) in heart tissues from sham and T2DM mice in both *Otud7b*$^{fl/fl}$ and *Otud7b* CKO groups. **g** The mRNA levels of *Tnfa*, *Il6*, *Cxcl10*, and *Ccl22* in heart tissues. **h** The mRNA levels of *Fas* and *Fasl* were quantified by RT-qPCR in heart tissues from the indicated groups. **i** Representative images of TUNEL staining (red) in heart tissues. **j** Representative immunofluorescence images of cleaved-caspase 3 (green) in heart tissues. **k** Neonatal rat primary cardiomyocytes (NRPCs) were transfected with His-TAK1-WT and His-TAK1-K346R plasmids, and the OTUD7b was silenced using siOTUD7b, then the NRPCs were exposed to high glucose (HG; 33 mM) and palmitic acid (PA; 100 μM). The mRNA levels of *Fas*, *Fasl*, *Tnfa* and *Il6* were detected. For **i**, scale bar = 50 μm. For **j**, scale bar = 100 μm. Data are shown as mean ± SEM; **a**–**e**, **k** $n = 3$; **f**–**j** $n = 6$; For **g**, **h**, **k**, *P* values were determined by one-way ANOVA followed by Tukey *post hoc* tests; For **g** (*Tnfa*), *P* values were determined by Welch's ANOVA with Dunnett's T3 *post hoc* test. *P* values indicated.

TAK1-K346 ubiquitination is essential for OTUD7b deficiency-mediated cardiac protection in DCM

To validate the positive role of OTUD7b-mediated deubiquitination at TAK1 K346 on DCM, we established recombinant adeno-associated virus serotype 9 (AAV9) vectors expressing either wild-type TAK1 or TAK1-K346R mutant (TAK1^{K346R}) under the cardiomyocyte-specific cTnT promoter. These vectors were delivered via tail vein injection to *Otud7b* CKO and *Otud7b*$^{fl/fl}$ mice, followed by HFD/STZ administration two weeks later (Fig. 8a). We confirmed that OTUD7b expression was successfully lowered in the hearts of *Otud7b* CKO mice. Compared with the AAV9-TAK1 group, the AAV9-TAK1^{K346R} group showed elevated levels of both TAK1 and p-TAK1, whereas the ratio of p-TAK1 to TAK1 remained unchanged (Figs. 8b and S11a). These results indicate that the TAK1^{K346R} mutation enhances TAK1 protein stability without affecting its kinase activity. As expected, neither TAK1 nor TAK1^{K346R} overexpression in cardiomyocytes altered hyperglycemia or body weight gain in T2DM mice (Fig. 8c, d). Importantly, TAK1^{K346R} exacerbated diabetes-induced cardiac injury, including cardiac dysfunction, hypertrophy, and fibrosis, and OTUD7b deficiency failed to alleviate the cardiac damage in AAV9-TAK1^{K346R} mice (Figs. 8e–l, and S11b, c; Supplementary Table 5). Consistently, TAK1^{K346R} further increased cleaved-caspase 3^{+} cells, caspase 8 activity, and inflammatory gene expression, compared to wild-type TAK1 in diabetic hearts, and OTUD7b deficiency also failed to attenuate these parameters induced by TAK1^{K346R} (Fig. S12a–d). These data suggest that K346 ubiquitination of TAK1 is essential for *Otud7b* CKO-mediated protection against DCM.

DISCUSSION

Our study unveils a previously unrecognized pathogenic axis centered on the cardiomyocyte-specific deubiquitinase OTUD7b in the progression of DCM. We demonstrate that OTUD7b is selectively upregulated in diabetic hearts and that its genetic ablation in cardiomyocyte-specific knockout mouse models of both T1DM and T2DM confers robust protection against diabetes-induced cardiac dysfunction, hypertrophy, and fibrosis. This protection is mechanistically linked to the attenuation of apoptosis and inflammation, processes governed by the TAK1-MAPK signaling pathway. Mechanistically, OTUD7b interacts with TAK1 via its ZF domain and specifically removes K48-linked polyubiquitin chains from K346 of TAK1. This action stabilizes TAK1 by blocking its proteasomal degradation, thereby enhancing the protein levels of both TAK1 and p-TAK1. Importantly, overexpression of the TAK1-K346R mutant completely abolished the cardioprotective effects of OTUD7b deficiency. Therefore, we propose the OTUD7b-TAK1 axis as a central molecular mechanism mediating DCM pathogenesis, offering a novel therapeutic target for intervention. The key mechanism finding is summarized in the Graphical Abstract.

Mounting evidence indicates that DUBs play critical yet context-dependent roles in the pathogenesis of DCM. Previously, USP28 has been shown to safeguard mitochondrial function and cardiac contractility in DCM, and it has been reported that USP13 ameliorates DCM by suppressing NLRP3-mediated pyroptosis [25, 35]. However, some DUBs can also exert detrimental effects, as our previous work demonstrated that OTUD1 promotes DCM progression [5]. These findings collectively highlight the therapeutic potential of DUBs and suggest that targeting specific DUBs may offer novel avenues for DCM intervention. Within this context, our study identifies a new DUB, OTUD7b, as a key pathological driver in the heart. Intriguingly, OTUD7b has been reported to exert protective roles in pressure-overload-induced cardiac hypertrophy by stabilizing factors such as KLF4 and HNF4α [23, 24]. This functional switch underscores how differing etiologies (e.g., mechanical stress vs. metabolic toxicity) reprogram DUB substrate specificity and functional output in a microenvironment-dependent manner. Although OTUD7b is expressed at low levels in fibroblasts and immune cells, our cardiomyocyte-specific knockout model confirms that the observed cardiac protection is primarily mediated by cardiomyocyte-autonomous effects. Thus, cardiomyocyte OTUD7b emerges as a key pathological driver in the metabolically stressed milieu of DCM. This context-dependent role further emphasizes the therapeutic window of selectively inhibiting OTUD7b for DCM treatment.

DUBs execute their regulatory roles primarily through deubiquitinating specific substrate proteins. OTUD7b is known to target diverse substrates such as RIPK1 [22], β-catenin [36], and SQSTM1/p62 [37] in distinct cells and pathological settings. Here, we identified TAK1 as a novel and critical substrate of OTUD7b in cardiomyocytes. This finding holds substantial pathophysiological relevance, as sustained hyperglycemia drives aberrant TAK1 activation, contributing to irreversible myocardial damage in advanced DCM, whereas suppression of TAK1 has been established as a protective strategy against DCM [13, 14]. Through functional validation, we demonstrate that forced overexpression of TAK1 completely rescues diabetic cardiac injury in OTUD7b-deficient models, confirming TAK1 as the principal downstream effector of OTUD7b's detrimental role in DCM. As a central regulator of pro-apoptotic and pro-inflammatory signaling, TAK1 activation engages the MAPK pathway; accordingly, our transcriptomic and experimental data show that OTUD7b deficiency suppresses MAPK signaling, attenuating both extrinsic apoptosis and inflammation in the diabetic hearts, which is consistent with the reported role of the TAK1-JNK/p38 axis in promoting apoptosis during ischemia-reperfusion injury [27, 38]. Mechanistically, OTUD7b acts as a molecular amplifier that deubiquitinates and stabilizes TAK1 in cardiomyocytes, thereby exacerbating pathological downstream

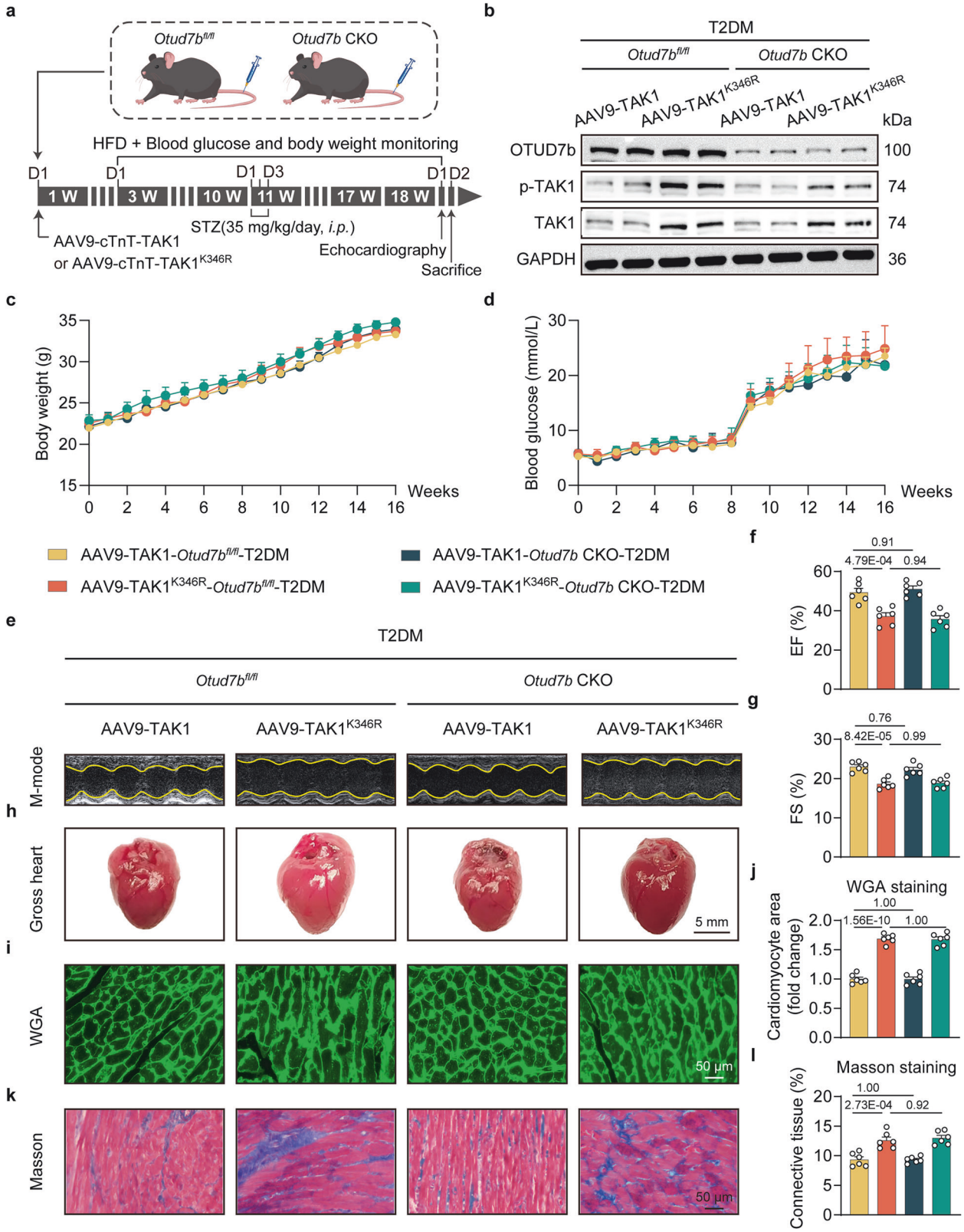

cascades. Importantly, because TAK1 is indispensable for physiological cell survival and immune homeostasis, its broad pharmacological inhibition risks severe off-target effects such as PANoptosis [33, 39]. However, our data showed that OTUD7b expression was very low in normal physiological hearts, and OTUD7b knockout did not induce any side effects in control mouse hearts. It may indicate that OTUD7b is a pathological target for DCM. Therefore, compared to directly targeting TAK1 kinase activity by small-molecule inhibitors, we propose a precise and safe TAK1-inhibiting strategy through targeting OTUD7b under pathological conditions. By

Fig. 8 TAK1-K346 ubiquitination is essential for OTUD7b deficiency-mediated cardiac protection in DCM. a Schematic representation of the experimental design. Adeno-Associated Virus 9 (AAV9) vectors carrying TAK1 (AAV9-cTnT-TAK1) and TAK1-K346R (AAV9-cTnT-TAK1^{K346R}) with the cardiomyocyte-specific promoter cTnT were administered to both *Otud7b*$^{fl/fl}$ and *Otud7b* CKO mice via tail vein injection. After 2 weeks, mice were induced to T2DM by low-dose streptozotocin (STZ, 35 mg/kg) administration for 3 days, combined with high-fat diet (HFD) feeding for 16 weeks. **b** Western blot analysis of OTUD7b, TAK1 and p-TAK1 in heart tissues. **c**, **d** Blood glucose levels and body weight of mice were measured. **e** Representative M-mode echocardiographic images of the indicated group. **f**, **g** Values of ejection fraction (EF%) and fractional shortening (FS%) by echocardiography. **h** Representative images of the whole heart. **i**, **j** Wheat germ agglutinin (WGA) staining and quantitative analysis in heart sections. **k**, **l** Representative images and quantification of Masson's Trichrome staining in heart tissues. For **h**, scale bar = 5 mm; For **i**, **k**, scale bar = 50 μm. Data are shown as mean ± SEM; $n = 6$. *P* values were determined by one-way ANOVA followed by Tukey *post hoc* tests. *P* values indicated.

specifically inhibiting the protein-protein interaction interface (e.g., via the OTUD7b ZF domain) or the catalytic pocket of OTUD7b, it may be possible to selectively abrogate the pathological stabilization of TAK1 in DCM while preserving its essential physiological functions, thereby optimizing both therapeutic efficacy and safety for DCM treatment.

The activity and stability of TAK1 are precisely regulated by a sophisticated network of PTMs, including phosphorylation, ubiquitination, acetylation, and methylation [15, 40–42]. Phosphorylation of its activation loop serves as a direct hallmark of its activation status [40]. In addition to phosphorylation, ubiquitination plays an especially pivotal and bidirectional regulatory role in TAK1 regulation. Distinct polyubiquitin linkage types exert opposing effects on the fate and function of TAK1. On one hand, K63-linked polyubiquitination is widely recognized as a key positive signal for TAK1 activation through indirectly regulating TAK1 phosphorylation. For example, upon inflammatory stimulation, K63-linked polyubiquitination at K158 of TAK1 is crucial for its recruitment to signaling complexes and subsequent phosphorylation [43, 44]. Recent studies have also identified K562 as another K63-linked ubiquitination site, further underscoring the prevalence of this modification in initiating TAK1 activity [45]. The deubiquitinase USP4 was found to downregulate TAK1 activity by cleaving its K63-linked chains [30, 45]. On the other hand, K48-linked polyubiquitination typically targets TAK1 for proteasomal degradation, thereby constituting a critical negative feedback mechanism [29, 30]. To date, several lysine residues, including K72, K346, and K547, have been identified as potential sites for K48-linked polyubiquitination of TAK1 [29–32]. Here, we demonstrate that OTUD7b selectively binds to TAK1 and removes K48-linked polyubiquitin chains from K346, thereby blocking the proteasomal degradation of TAK1. Strikingly, the K346R mutation increased TAK1 stability and further exacerbated diabetes-induced cardiac injury, confirming the functional importance of this site.

Several limitations of this study should be acknowledged. The K346R rescue experiment was performed only in the T2DM model, as it represents the majority of clinical DCM cases; an extension to T1DM would further strengthen generalizability. All animal experiments used male mice exclusively, leaving potential sex-dependent differences unexplored. Additionally, human cardiac tissue samples were not available to examine OTUD7b expression in DCM patients, warranting future clinical validation.

In conclusion, this study demonstrates that in DCM, cardiomyocyte-specific OTUD7b drives myocardial apoptosis, inflammation, and subsequent cardiac remodeling by deubiquitinating and stabilizing TAK1 at the K346 site, leading to overactivation of the TAK1-MAPK pathway. This discovery not only provides a fresh molecular perspective on DCM pathology but also nominates OTUD7b itself or the OTUD7b-TAK1 interaction as a promising target for therapeutic intervention. Future development of specific small-molecule inhibitors or peptide-based disruptors based on the OTUD7b-TAK1 axis holds significant translational potential for DCM treatment.

DATA AVAILABILITY

All data included within the article, or Supplementary Information, are available from the authors on request.

ACKNOWLEDGEMENTS

The authors acknowledge the support from the Scientific Research Center, Hangzhou Medical College, and Liwei, Laboratory Animal Center of Zhejiang University, for her assistance in animal experiments.

AUTHOR CONTRIBUTIONS

GL, HZY, WBJ and XH contributed to the conception and design of the study. XH, GXL, JNZ, MYH, LZ, and JJZ contributed to the methodology. GXL and ZPZ performed the investigation. JT, ZQH, YRW, TQZ, NZ and JLM performed data curation. GL, HZY, and XH supervised the study. XH and GXL wrote the original draft. XH and QJS acquired funding. All authors reviewed and approved the final manuscript.

FUNDING

This work was supported by the National Natural Science Foundation of China (grant no. U24A20814 to GL), the Zhejiang Provincial Traditional Chinese Medicine Science and Technology Program Project (grant no. 2026ZL0088 to XH), the Natural Science Foundation of Zhejiang Province (grant no. TGD24C040023 to QJS), the Medical Scientific Research Foundation of Zhejiang Province (grant no. 2024KY932 to XH), and the Basic Scientific Research Funds of the Department of Education of Zhejiang Province (Grants No. KYZD2025004 to XH).

ADDITIONAL INFORMATION

Supplementary information The online version contains supplementary material available at https://doi.org/10.1038/s41401-026-01891-w.

Competing interests: The authors declare no competing interests.

REFERENCES

1. Tan Y, Zhang Z, Zheng C, Wintergerst KA, Keller BB, Cai L. Mechanisms of diabetic cardiomyopathy and potential therapeutic strategies: preclinical and clinical evidence. Nat Rev Cardiol. 2020;17:585–607.
2. Bugger H, Abel ED. Molecular mechanisms of diabetic cardiomyopathy. Diabetologia. 2014;57:660–71.
3. Huo JL, Feng Q, Pan S, Fu WJ, Liu Z, Liu Z. Diabetic cardiomyopathy: early diagnostic biomarkers, pathogenetic mechanisms, and therapeutic interventions. Cell Death Discov. 2023;9:256.
4. Zhao X, Liu S, Wang X, Chen Y, Pang P, Yang Q, et al. Diabetic cardiomyopathy: clinical phenotype and practice. Front Endocrinol. 2022;13:1032268.
5. Han X, Zheng R, Zhang J, Liu Y, Li Z, Liu G, et al. Cardiomyocyte OTUD1 drives diabetic cardiomyopathy via directly deubiquitinating AMPKα2 and inducing mitochondrial dysfunction. Nat Commun. 2025;16:6668.
6. Zhang M, Sui W, Xing Y, Cheng J, Cheng C, Xue F, et al. Angiotensin IV attenuates diabetic cardiomyopathy via suppressing FoxO1-induced excessive autophagy, apoptosis and fibrosis. Theranostics. 2021;11:8624–39.
7. Zhang H, Ge S, He K, Zhao X, Wu Y, Shao Y, et al. FoxO1 inhibits autophagosome-lysosome fusion leading to endothelial autophagic-apoptosis in diabetes. Cardiovasc Res. 2019;115:2008–20.
8. Mann DL. Inflammatory mediators and the failing heart: past, present, and the foreseeable future. Circ Res. 2002;91:988–98.
9. Swirski FK, Nahrendorf M. Cardioimmunology: the immune system in cardiac homeostasis and disease. Nat Rev Immunol. 2018;18:733–44.

10. Han X, Zhou W, Zhang J, Tu Y, Wei J, Zheng R, et al. Linderalactone mitigates diabetic cardiomyopathy in mice via suppressing the MAPK/ATF6 pathway. Int Immunopharmacol. 2023;124:110984.
11. Suetomi T, Miyamoto S, Brown JH. Inflammation in nonischemic heart disease: initiation by cardiomyocyte CaMKII and NLRP3 inflammasome signaling. Am J Physiol Heart Circ Physiol. 2019;317:H877–90.
12. Ma M, Dang Y, Chang B, Wang F, Xu J, Chen L, et al. TAK1 is an essential kinase for STING trafficking. Mol Cell. 2023;83:3885–903.e5.
13. Jin B, Wang J, Chen Y, Zuo W, Hong B, Li J, et al. Focal adhesion kinase induces cardiac remodeling through NF-κB-mediated inflammatory responses in diabetic cardiomyopathy. Int Immunopharmacol. 2023;120:110280.
14. Banerjee A, Singla DK. MSC exosomes attenuate sterile inflammation and necroptosis associated with TAK1-pJNK-NFKB mediated cardiomyopathy in diabetic ApoE KO mice. Front Immunol. 2024;15:1348043.
15. Zhao Y, Fan S, Zhu H, Zhao Q, Fang Z, Xu D, et al. Podocyte OTUD5 alleviates diabetic kidney disease through deubiquitinating TAK1 and reducing podocyte inflammation and injury. Nat Commun. 2024;15:5441.
16. Sun T, Liu Z, Yang Q. The role of ubiquitination and deubiquitination in cancer metabolism. Mol Cancer. 2020;19:146.
17. Xiao X, Shi J, He C, Bu X, Sun Y, Gao M, et al. ERK and USP5 govern PD-1 homeostasis via deubiquitination to modulate tumor immunotherapy. Nat Commun. 2023;14:2859.
18. Hu H, Brittain GC, Chang JH, Puebla-Osorio N, Jin J, Zal A, et al. OTUD7B controls non-canonical NF-κB activation through deubiquitination of TRAF3. Nature. 2013;494:371–4.
19. Ding C, Cao L, Wang R, Wu Q, Li M, Zhang J, et al. OTUD7B is a new deubiquitinase targeting p53. Theranostics. 2025;15:2121–38.
20. Wang B, Jie Z, Joo D, Ordureau A, Liu P, Gan W, et al. TRAF2 and OTUD7B govern a ubiquitin-dependent switch that regulates mTORC2 signalling. Nature. 2017;545:365–9.
21. Zhang B, Yang C, Wang R, Wu J, Zhang Y, Liu D, et al. OTUD7B suppresses Smac mimetic-induced lung cancer cell invasion and migration via deubiquitinating TRAF3. J Exp Clin Cancer Res. 2020;39:244.
22. Harit K, Yi W, Jeron A, Schmidt J, Beckervordersandforth R, Wyler E, et al. Astrocytic-OTUD7B ameliorates murine experimental autoimmune encephalomyelitis by stabilizing glial fibrillary acidic protein and preventing inflammation. Nat Commun. 2025;16:9279.
23. Zheng R, Song W, Wang C, Du X, Liu C, Sun X, et al. Deubiquitinase OTUD7B stabilizes HNF4α to alleviate pressure overload-induced cardiac hypertrophy by regulating fatty acid oxidation and inhibiting ferroptosis. Biomark Res. 2025;13:53.
24. Du BB, Zhang JL, Kong LY, Shi HT, Zhang DH, Wang X, et al. Ovarian tumor domain-containing 7B attenuates pathological cardiac hypertrophy by inhibiting ubiquitination and degradation of krüppel-like factor 4. J Am Heart Assoc. 2023;12:e029745.
25. Xie SY, Liu SQ, Zhang T, Shi WK, Xing Y, Fang WX, et al. USP28 serves as a key suppressor of mitochondrial morphofunctional defects and cardiac dysfunction in the diabetic heart. Circulation. 2024;149:684–706.
26. Arrigo AB, Zhu W, Williams KA, Guzman-Moreno C, Lo C, Lin JHI. Contribution of LRP1 in human congenital heart disease correlates with its roles in the outflow tract and atrioventricular cushion development. Genes. 2023;14:947.
27. Zeng JJ, Shi HQ, Ren FF, Zhao XS, Chen QY, Wang DJ, et al. Notoginsenoside R1 protects against myocardial ischemia/reperfusion injury in mice via suppressing TAK1-JNK/p38 signaling. Acta Pharm Sin. 2023;44:1366–79.
28. Wu X, Liu S, Sagum C, Chen J, Singh R, Chaturvedi A, et al. Crosstalk between Lys63- and Lys11-polyubiquitin signaling at DNA damage sites is driven by Cezanne. Genes Dev. 2019;33:1702–17.
29. Fan Y, Shi Y, Liu S, Mao R, An L, Zhao Y, et al. Lys48-linked TAK1 polyubiquitination at lysine-72 downregulates TNFα-induced NF-κB activation via mediating TAK1 degradation. Cell Signal. 2012;24:1381–9.
30. Liang L, Fan Y, Cheng J, Cheng D, Zhao Y, Cao B, et al. TAK1 ubiquitination regulates doxorubicin-induced NF-κB activation. Cell Signal. 2013;25:247–54.
31. Qian H, Lu Z, Hao C, Zhao Y, Bo X, Hu Y, et al. TRIM44 aggravates cardiac fibrosis after myocardial infarction via TAK1 stabilization. Cell Signal. 2023;109:110744.
32. Wang L, Zhang X, Lin ZB, Yang PJ, Xu H, Duan JL, et al. Tripartite motif 16 ameliorates nonalcoholic steatohepatitis by promoting the degradation of phospho-TAK1. Cell Metab. 2021;33:1372–88.e7.
33. Malireddi RKS, Gurung P, Kesavardhana S, Samir P, Burton A, Mummareddy H, et al. Innate immune priming in the absence of TAK1 drives RIPK1 kinase activity-independent pyroptosis, apoptosis, necroptosis, and inflammatory disease. J Exp Med. 2020;217:jem.20191644.
34. Wang D, Li Y, Yang H, Shen X, Shi X, Li C, et al. Disruption of TIGAR-TAK1 alleviates immunopathology in a murine model of sepsis. Nat Commun. 2024;15:4340.
35. Xu D, Han J, Ye B, Lin L, Chen J, Jin Y, et al. USP13 ameliorates diabetic cardiomyopathy via deubiquitinating NLRP3 and inhibiting pyroptosis in cardiomyocytes. Cell Death Differ. 2025; 3:914–29.
36. Sun J, Jin X, Li Y. OTUD7B inhibited hepatic injury from NAFLD by inhibiting K48-linked ubiquitination and degradation of β-catenin. Biochim Biophys Acta Mol Basis Dis. 2025;1871:167555.
37. Xie W, Tian S, Yang J, Cai S, Jin S, Zhou T, et al. OTUD7B deubiquitinates SQSTM1/p62 and promotes IRF3 degradation to regulate antiviral immunity. Autophagy. 2022;18:2288–302.
38. Kang Z, Yang M, Liu Y, Gui Y, Dong Y, Zhou H, et al. Myocardial mitochondrial antiviral signaling protein promotes heart Ischemia-reperfusion injury via RIG-I signaling in mice. Nat Commun. 2025;16:5101.
39. Malireddi RKS, Kesavardhana S, Kanneganti TD. ZBP1 and TAK1: master regulators of NLRP3 inflammasome/pyroptosis, apoptosis, and necroptosis (PAN-optosis). Front Cell Infect Microbiol. 2019;9:406.
40. Hirata Y, Takahashi M, Morishita T, Noguchi T, Matsuzawa A. Post-translational modifications of the TAK1-TAB complex. Int J Mol Sci. 2017;18:205.
41. Paquette N, Conlon J, Sweet C, Rus F, Wilson L, Pereira A, et al. Serine/threonine acetylation of TGFβ-activated kinase (TAK1) by Yersinia pestis YopJ inhibits innate immune signaling. Proc Natl Acad Sci USA. 2012;109:12710–5.
42. Zhang L, Ding X, Cui J, Xu H, Chen J, Gong YN, et al. Cysteine methylation disrupts ubiquitin-chain sensing in NF-κB activation. Nature. 2011;481:204–8.
43. Fan Y, Yu Y, Mao R, Zhang H, Yang J. TAK1 Lys-158 but not Lys-209 is required for IL-1β-induced Lys63-linked TAK1 polyubiquitination and IKK/NF-κB activation. Cell Signal. 2011;23:660–5.
44. Li Q, Yan J, Mao AP, Li C, Ran Y, Shu HB, et al. Tripartite motif 8 (TRIM8) modulates TNFα- and IL-1β-triggered NF-κB activation by targeting TAK1 for K63-linked polyubiquitination. Proc Natl Acad Sci USA. 2011;108:19341–6.
45. Chen IT, Hsu PH, Hsu WC, Chen NJ, Tseng PH. Polyubiquitination of transforming growth factor β-activated kinase 1 (TAK1) at lysine 562 residue regulates TLR4-mediated JNK and p38 MAPK activation. Sci Rep. 2015;5:12300.